

See discussions, stats, and author profiles for this publication at: <https://www.researchgate.net/publication/265244067>

Modeling Identification and Control of Air Pre-heating Furnace of a Pneumatic Conveying and Drying Process

ARTICLE in INDUSTRIAL & ENGINEERING CHEMISTRY RESEARCH · AUGUST 2014

Impact Factor: 2.59 · DOI: 10.1021/ie501124s

CITATIONS

2

READS

89

3 AUTHORS, INCLUDING:



[Biplab Satpati](#)

University of Burdwan

9 PUBLICATIONS 16 CITATIONS

[SEE PROFILE](#)



[Chiranjib Koley](#)

National Institute of Technology, Durgapur

15 PUBLICATIONS 16 CITATIONS

[SEE PROFILE](#)

Modeling Identification and Control of an Air Preheating Furnace of a Pneumatic Conveying and Drying Process

Biplab Satpati,[†] Chiranjib Koley,^{*,‡} and Subhashis Datta[§]

[†]Electrical Engineering Department, University Institute of Technology, Burdwan, West Bengal 713104, India

[‡]Electrical Engineering Department, National Institute of Technology, Durgapur, West Bengal 713209, India

[§]Mechanical Engineering Department, Ghani Khan Choudhury Institute of Engineering & Technology, Malda, West Bengal 732144, India

Supporting Information

ABSTRACT: The present work uses a scale down industrial pneumatic conveying and drying system in order to develop control-oriented models and suitable robust control strategies for the air preheating furnace of the system. A better control system has been achieved by utilizing the benefits of integrating first principle models, system identification techniques and parametric robust control methods. Though these processes are widely used in drying and transmission of different food, pharmaceutical and industrial products in the form of powder like fine-grained material, but suitable control oriented thermal models for these processes have not been studied. In the work the air preheating furnace of a pneumatic conveying and drying system is initially modeled with first principles. The novel dynamic models derived from first-principles is intended to evaluate dynamic changes in outlet air temperature corresponds to changes in current input to heating coils, air flow velocity and ambient temperature. Then a continuous time (CT) data driven model identification technique based on Simplified Refined Instrumental Variable (SRIV) approach has been applied in order to identify the model parameters as per the desired structures. The identified systems were then validated with different sets of experimental data, and found to be closely correlated. Finally a novel robust control law i.e. refined particle swarm optimization (PSO) enabled automated Quantitative Feedback Theory (QFT) (refined PSO-QFT) has been proposed and implemented in order to improve the temperature control system of the pneumatic conveying and drying process.

1. INTRODUCTION

The applications of pneumatic conveying and drying systems are wide in various industries, such as for pulverized coal and ash handling in power plants,^{1,2} sawdust for pellet production,³ calcinations of gypsum,^{4,5} cement production,^{6,8} and food and pharmaceutical product processing.^{9,14} Especially in the food industries, pneumatic conveying and drying has become very popular for batch production or the processing of agro-based food products such as wheat, corn, turmeric, tea, and coffee etc. because of its simplicity in construction, efficiency in terms of operations, and environmental and economical aspects as compared to other conveying and drying units.^{9,11,14}

The drying operation in these units is characterized by a coherent flow of a preheated gas–grain mix, in which grains are dehydrated or dried by the preheated air during transportation through the air duct, and thereafter the grains are separated according to size by some cyclone systems. There has been enormous research work in the broad area of pneumatic conveying and powder technology.^{1–20} In convective drying, air temperature, relative humidity, and velocity have a significant effect on the drying kinetics and quality of food products.^{11–14} Since the preheating of air before mixing with wet material improves the overall performance, reducing energy consumption and drying time,²¹ most pneumatic convective dryers use an air preheater. In a majority of the applications, the outlet air temperature of the air preheater is dynamically controlled according to the airflow rate, as required for the sustained conveyance of materials and moisture content of the input raw

material, so that the moisture content of the final product remains within the desired limits; however, the airflow rate is mainly governed by the inlet wet material flow rate and moisture content. In the pneumatic conveying and drying process, the mass flow rate of the input raw materials, their moisture content, and their grain size often vary during operation, therefore the desired set points of the temperature and airflow controller need to be dynamically altered according to the process input conditions. Unlike the relatively faster airflow control of the process, duct air-temperature control is more critical, because of the large time constants of the heating system employed and the dependency of the preheated air temperature on the airflow rate. Further, the different time-constants at different operating region make the existing PID control inefficient in providing a fast response in the dynamical varying load situation. One of the first papers to address the problem of controlling the air temperature of the dryer through an appropriate signal to the thyristor-controlled heater is by Garcia et al.²² The work demonstrates that the fixed gain feedback controllers (PID) are insufficient to compensate for

Special Issue: Energy System Modeling and Optimization Conference 2013

Received: March 18, 2014

Revised: August 22, 2014

Accepted: August 24, 2014

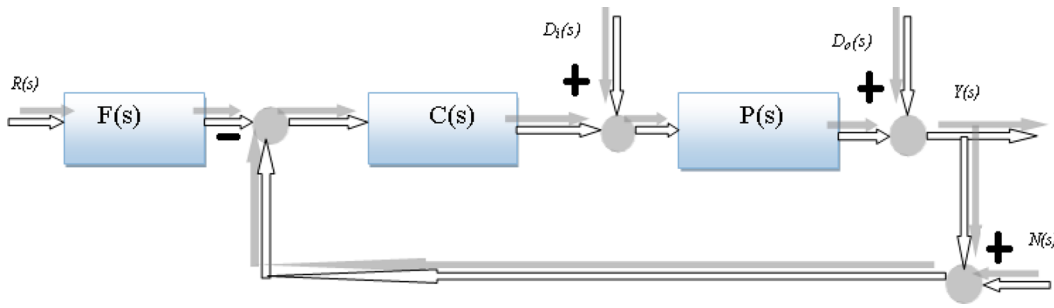


Figure 1. 2-DOF feedback control system.

parameter variations in the plant as well as to adapt the changes in the process environment. Moreover furnace temperature control processes generally contain some inbuilt nonlinearities like static actuator nonlinearity, output saturation of the final control element, and dead zones in the process dynamic characteristics. Apart from plant parametric variations some unstructured uncertainties like stochastic disturbances, measurement errors, and process noises may also be introduced into the process during its operations. Thus, to obtain robust and tight control performance, the controllers have to be synthesized using model based control (MBC) techniques. But without an *a priori* model it is difficult to develop a MBC scheme. Therefore, to improve the air temperature control system, a robust current control law based on the mathematical model must be implemented, which is needed to deal with the stringent specifications and dynamic operating conditions of the duct air temperature control process.

There has been much research on mathematical model identification of boiler,²³ gas fired furnace,²⁴ room heating/HVAC system,^{25,26} solar heating system,²⁷ vapor compression system of air conditioner,²⁸ synchronous generator,²⁹ two level quantum systems,³⁰ multiple motor drive system,³¹ wastewater system,³² laser welding process,³³ stirred tank heater,³⁴ various industrial processes,³⁵ industrial crystallizer train for para-xylene recovery,³⁶ flow control valve friction,³⁷ ceramic tiles cooling process,³⁸ industrial heating process,³⁹ flotation column,⁴⁰ steel pickling process,⁴¹ etc., while much less attention has been paid for developing mathematical models of air preheating systems as widely used in food processing and drying of materials in powder form. Though some of the works address heat transfer and kinetic drying of a convective pneumatic dryer highlighting the experimental and numerical solutions,^{42–44} these works intended to neither develop a dynamic thermal model of the dryer nor implement model-based control techniques. Moreover, there are only a few mathematical models (electric heating furnace) available, most of which are based on computational fluid dynamics (CFD) or magneto-hydrodynamics (MHD) modeling techniques.^{45,46} While these models can offer detailed predictions of the fluid flow, heat transfer, and electric fields in the furnaces, they models are not control oriented. However, most of the research^{42–46} still focuses on understanding the drying mechanisms and product quality, rather than on improving the control mechanism.

In a complex process such as a pneumatic conveying and drying system difficulties are often encountered in identification of models under various flow settings and operational and environmental conditions. Not only that, it is even more difficult for the designed controller to ensure the requisite tracking performance and disturbance rejection over the entire operating region. Hence the system under investigation

requires a controller, which should be capable of handling all the variations in process parameters for the entire performance envelope of operation and at the same time must ensure a proper trade-off between stability, performance, and disturbance rejection specifications. As suggested by the various literature of the parametric robust control approach,⁴⁷ among the various robust control methods, quantitative feedback theory (QFT)^{48,49} has attained an impressive level of acceptability and success in diverse application areas like flight control,^{50–52} marine control,^{53–55} missile control,^{56–58} power systems and power electronics applications,^{59–62} robot manipulator control,⁶³ and process control applications,^{64–66} particularly when the plant becomes large, distributed, and highly uncertain. The QFT method offers a number of advantages compared to other robust control methods such as the ability to provide a lowest order compensator, one design for the full envelop, cost of feedback can be controlled, controller synthesized for the exact amount of plant uncertainty, computationally less intensive, etc.^{48,49} These are the main motivations behind applying QFT in the proposed application.

The graphical loop shaping performed by using the QFT tool box⁶⁷ involves a trial and error procedure, and also the success of the design depends, to a large extent, on the experience of the designer. That is why for the last decade, research is more concentrated on the development of the automatic loop-shaping algorithm.^{68–81} A significant amount of research has been reported so far in this particular area in the framework of soft computing^{55,72,79–81} interval constraint analysis,^{74,78} linear programming,^{69,70} crone structures,⁷³ and hybrid optimization techniques.⁷⁶ In the present contribution the PSO-enabled QFT^{55,79,80} method has been used for loop shaping, but the algorithm is being improved to a large extent by considering some adaptive modifications in the penalty functions involved with the multi-objective linear constraint optimization problem.

Therefore, the present work focuses on deriving suitable mathematical as well as data-driven models, followed by designing and implementing a robust current control law by using a refined PSO-enabled automated QFT (refined PSO-QFT) method for improved drying and conveying of the process under consideration.

2. THEORETICAL BACKGROUND OF CONTROL DESIGN METHOD

This section gives an overview of quantitative feedback theory (QFT) and particle swarm optimization (PSO) technique.

2.1. QFT Overview. QFT is a unified frequency domain technique utilizing the Nichols chart (NC) for achieving the desired robust design over a specified region of plant uncertainty. This method was created and developed by Prof.

I. M. Horwitz.⁴⁸ It is now recognized as a well established method for design of robust controllers for the plant with large classes of uncertainties, output/input disturbances, and noises. The true importance of feedback is in “achieving desired performance despite uncertainty”. If so, then the actual design and the cost of feedback should be closely related to the extent of the uncertainty and to the narrowness of the performance tolerances. In short, it should be quantitative. Basically, the QFT design is based upon (i) specifying the tolerances in frequency domain (time domain tolerances should be converted into corresponding frequency domain tolerances) by means of set of plant transfer functions and closed loop control ratios and (ii) determining the loop transmission functions and prefilter functions to satisfy the various resulting bounds corresponding to the tolerances.

A single-loop two-degree of freedom (DOF) feedback control structure (providing freedom to shape the feedback and tracking responses independently) is shown in Figure 1. Where $C(s)$ is the cascade compensator, and $F(s)$ is an input prefilter. Here, \mathcal{P} is the plant uncertainty given by $\text{Pe}\{P(s, \Delta); \Delta\epsilon\lambda\}$, where $\lambda \in \mathbb{R}^l$ is a vector of plant parameters whose values vary over a parametric box Δ given by

$$\Delta = \{\lambda \in \mathbb{R}^l : \lambda_i \in [\lambda_i^{\min}, \lambda_i^{\max}], i = 1, 2, \dots, l\} \quad (1)$$

The open loop transmission function is defined as

$$L(s, \Delta) = C(s)P(s, \Delta) \quad (2)$$

$$L(j\omega, \Delta) = C(j\omega) e^{j\varphi(j\omega)} P(j\omega) e^{j\theta(j\omega)} \quad (3)$$

The nominal loop transmission function is

$$L_0(j\omega, \Delta) = C(j\omega) e^{j\varphi(j\omega)} P_0(j\omega) e^{j\theta(j\omega)} = l_0(j\omega) e^{j\psi_0(j\omega)} \quad (4)$$

where

$$l_0(j\omega) = C(j\omega) P_0(j\omega) \quad \text{and} \quad \psi_0(j\omega) = \varphi_0(j\omega) + \theta_0(j\omega) \quad (5)$$

In QFT compensator $C(s)$ is to be designed so that the variation of $R(s)$ to the uncertainty in the plant \mathcal{P} is within allowable tolerances, the robustness criteria is ensured and the disturbance-rejection requirement is met. In addition, the prefilter properties of $F(s)$ must be designed to tailor the responses to meet the tracking specification requirements.^{48,49} In general the following specifications are considered in QFT:

(a) Robust stability margin

$$\left| \frac{L(j\omega)}{1 + L(j\omega)} \right| \leq \mu \quad (6)$$

where μ is the supermom value of robust stability specification. The specification can be converted in terms of quadratic inequalities as follows:

$$c^2 p^2 \left(1 - \frac{1}{\mu^2} \right) + 2cp \cos(\psi + \theta) + 1 \geq 0 \quad (7)$$

where c and p are the magnitude of the controller and plant, respectively.

(b) Robust input disturbance rejection

$$\left| \frac{P(j\omega)}{1 + L(j\omega)} \right| \leq W_{d_i}(\omega) \quad (8)$$

$$c^2 p^2 + 2cp \cos(\psi + \theta) + \left(1 - \frac{p^2}{W_{d_i}^2} \right) \geq 0 \quad (9)$$

where $W_{d_i}(\omega)$ is the input disturbance specification.

(c) Control effort constraint

$$\left| \frac{C(j\omega)}{1 + L(j\omega)} \right| \leq W_C(\omega) \quad (10)$$

$$c^2 p^2 + 2cp \cos(\psi + \theta) + \left(1 - \frac{c^2}{W_C^2} \right) \geq 0 \quad (11)$$

where $W_C(\omega)$ is the control effort specification.

Robust tracking performance specification

$$|T_L(j\omega)| \leq \left| \frac{F(j\omega)L(j\omega)}{1 + L(j\omega)} \right| \leq |T_U(j\omega)| \quad (12)$$

where $T_L(j\omega)$ and $T_U(j\omega)$ are the lower and upper tracking performance specifications.

$$c^2 p_k^2 p_i^2 \left(1 - \frac{1}{\delta^2(\omega)} \right) + 2cp_k p_i \left[p_k \cos(\psi + \theta_i) - \frac{p_i}{\delta^2(\omega)} \cos(\psi + \theta_k) \right] + \left(p_k^2 - \frac{p_i^2}{\delta^2(\omega)} \right) \geq 0 \quad (13)$$

(e) Robust output disturbance rejection

$$\left| \frac{1}{1 + L(j\omega)} \right| \leq W_{d_o}(\omega) \quad (14)$$

$$c^2 p^2 + 2cp \cos(\psi + \theta) + \left(1 - \frac{1}{W_{d_o}^2} \right) \geq 0 \quad (15)$$

The above constraints are to be satisfied $\forall \text{Pe}\{P(s, \Delta); \Delta\epsilon\lambda\}, \forall \omega \in \Omega$ depending upon the type of problem.

2.2. Brief Overview of PSO. The particle swarm optimization (PSO) is a population-based optimization tool, which was developed by Kennedy et al.⁸² motivated by the social behavior of bird flocking and fish schooling. Kennedy et al.⁸² demonstrated that the velocity and position of the particles can be updated with the following equations:

Velocity update:

$$V_i^{t+1} = QV_i^t + K_1 \text{rand}_1(X_{pbest} - X_i^t) + K_2 \text{rand}_2 d_2(X_{gbest} - X_i^t) \quad (16)$$

Position update:

$$X_i^{t+1} = X_i^t + \gamma V_i^{t+1} \quad (17)$$

where K_1 and K_2 are two positive constants, rand_1 and rand_2 are random numbers in the range $[0, 1]$, and Q is the inertia weight. X_i^t represents current position of the i th particle and V_i^t is its current velocity. The position of the particles are updated

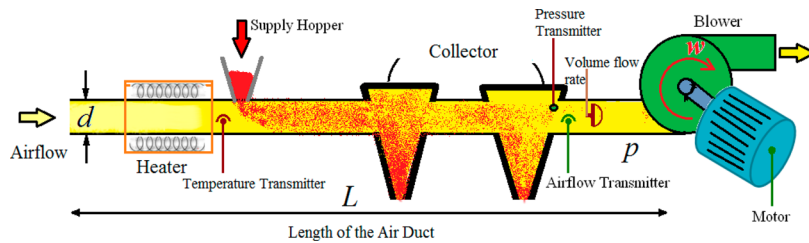


Figure 2. Schematic diagram of pneumatic conveying system.

using eq 17, where X_i^{t+1} is the new position of the i th particle at m -dimensional search space.

The weight Q is updated using the following equation:

$$Q = Q_{\max} - \left[\frac{Q_{\max} - Q_{\min}}{iter_{\max}} \right] iter \quad (18)$$

where $iter$ is the iteration count.

3. DESCRIPTION OF THE PROCESS MODEL

In the present framework a negative pressure closed-type typical pneumatic conveying system has been considered, which is commonly used for drying and separation of materials. A schematic block diagram of the system is shown in Figure 2. The duct of diameter d is used to convey material inserted through the hopper. A heater is used to heat the air to the desired temperature. A negative pressure is created inside the duct by the blower, so that the flow of air can carry the inserted material. The negative pressure is controlled by controlling the speed of the blower which basically controls the airflow rate through the duct and hence the amount of material to be conveyed and collected into the collectors. In order to maintain the material conveying process, the airflow rate through the duct is governed according to the mass flow rate of the supplied material through the hopper. The duct air is heated by the heater, the outlet air temperature of the heater needs to be controlled to obtain material of the desired moisture content, where the airflow rate and environmental temperature act as process disturbances.

A suitable laboratory scale model of the process has been implemented for the purpose of study, a laboratory scale model often found to be effective in the study of various control systems.^{28,30,32,33,83} The process flow and instrument diagram of the experimental setup is shown in Figure 3, which consists of the heating chamber, mixing chamber, blower, separators, and air duct.

A photograph of the experimental setup is shown in Figure S1 (Supporting Information). The outlet air temperature of preheater is measured by RTD sensor and controlled by controlling the current through the heating coil. A 3-Ph solid state relay (SSR) (model 25A, NIPONIX) is operated at high frequency in time proportional output (TPO) mode for controlling the heater current. The airflow rate and pressure inside the duct are measured by v-cone (Mc-crometer) and pressure transmitter (Honeywell, ST 3000) respectively, and is controlled by controlling the blower motor (3-ph induction type) through a variable frequency drive (VFD) (model IG5ASV01SIG5A-4, LG). Other parameters which are measured are the outside air temperature (RTD), pipe temperature (RTD), current through the heating coils (hall type), humidity, mixer load (hall type), etc. A distributed control system (DCS) (model HC 900, Honeywell) is used for

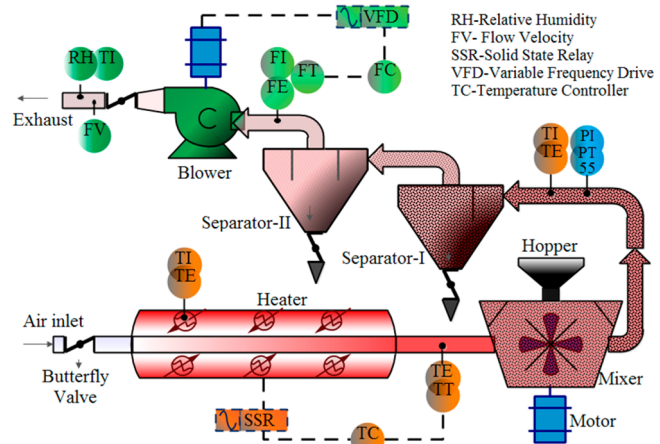


Figure 3. Process flow and instrument diagram.

monitoring and controlling the entire process. The PID control logic is implemented into the DCS through a functional logic diagram with the help of hybrid control designer (Honeywell) software (shown in Supporting Information Figure S2). For monitoring the process parameters and user interfaces supervisory control and data acquisition (SCADA) system of SpecView has been used (shown in Figure S2 [Supporting Information]).

The process is operated by controlling the outlet air temperature to some desired value, normally in the range of 40–90 °C, depending on the material to be processed and the air flow rate in the range of 100 to 1500 CFM. The outlet air temperature, airflow rate, and duct pressure are acquired by analog input (AI) channels of the DCS, and then sent to the respective PID controller, the output of the temperature PID controller is then sent to digital output (DO) port of the DCS through a TPO block, which then drives the SSR. The output of the airflow PID controller goes to the analog output (AO) port of the DCS, and is then converted into 4–20 mA current output, which finally goes to the variable frequency drive (VFD) for control of the blower speed. The heating chamber placed around the air duct increases the temperature of flowing air. The material to be processed is placed into the mixer grinder through the hopper and then conveyed by the hot air, for drying and heating. The final product is collected by the two cascaded cyclotron separators.

4. SYSTEM IDENTIFICATION

In this work, the time domain data driven system identification approach has been considered to obtain a proper set of model equations for the air preheater of the pneumatic conveying and drying system. The system identification can be divided into four steps: data collection with the help of suitable input, output design, selection of suitable model structure, model

parameter estimation, and model validation. A flow diagram of the system identification task, as considered in the work is presented in Figure 4.

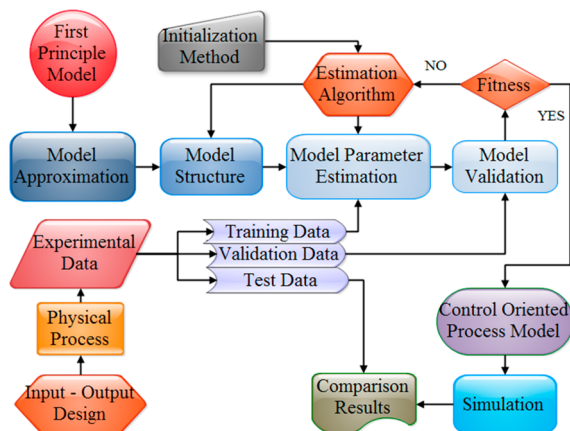


Figure 4. Flow diagram of proposed method.

4.1. Experiment Design and Data Collection. The purpose of performing the experiments is to obtain a set of linear models with the help of inputs (current through the heating coil, airflow rate and ambient temperature) and output (outlet air temperature). In the work, the effect of variation in one input to the output has been considered separately and independently. Therefore, the following set of measures has been taken before the experimental data was collected: (1) Both the PID controllers, that is, temperature PID and air flow PID, were kept in MANUAL mode and were operated at various manual settings; (2) the mixing motor was set to rotate at constant speed and at no-load; (3) loop rate/sampling frequency of the DCS was set to 1 Hz; (4) the cycle time for the TPO block was set to 10 s.

To collect a proper set of data which will be able to reflect system dynamics over the entire operating region, simultaneously maintaining other constraints such as safety, sensor span, and actuator saturation, etc., following set of experiments have been performed, which can be classified into four different modes. In mode-1, the current through the heating coil has been varied while the other two variables, that is, airflow rate and ambient temperature, are maintained to some fixed values. In this mode the current has been varied in different steps of variable amplitude and duration as shown in Figure 5a. The tests of mode-1 have been repeated for three different cases with airflow rate settings of 25% (lower), 50% (medium), and 75% (higher), and each case has been repeated three times, so that randomly chosen two data sets can be used in identification and validation while the remaining one can be used for independent testing. Input and output responses of the system for each of the three cases are presented in Figure 5 panels a, b, and c, respectively.

In mode-2, a similar kind of exercise has been performed, but in the cases of this mode the airflow rate has been varied while maintaining the current to fixed values so that it comes to different operating regions, that is, lower, medium and higher. Similar to mode-1, it also has three cases with fixed heater current settings of 30% (lower), 60% (medium), and 90% (higher) as shown in Figure 5, panels d, e, and f, respectively. While performing experiments in mode-1 and mode-2, the room air conditioners were maintained at a fixed temperature

so that the effect of ambient temperature variation on furnace outlet air temperature is minimized. In mode-3, the ambient temperature was varied in different operating regions for different fixed current and airflow rate settings by turning off the room air conditioners. Figure 5 panels g–i show such instances, where the variations of ambient temperature on furnace outlet air temperature are presented with airflow rate settings at 100%, 75%, and 25%, and current settings at 30%, 60%, and 90%, respectively. In mode 4, all the input variables have been varied; Figure 5j shows a section of such a test in which the room air-conditioners were turned off and the current and air flow rate was varied together. As mentioned in mode-1, all the experiments in the different cases of other modes were repeated three times. Before all the tests, the experimental model was used to run for at least 1 h to eliminate start up effects.

The recorded data as collected during the experiments in different modes were then preprocessed for the purpose of system identification, elimination of noises, and sensor artifacts. The heat energy supplied to the heater coil (Q) was computed by squaring the measured current data. It is to be noted here that the error involved in the measurement of current was significantly low, as it was estimated from the TPO-duty cycle of PLC, which generates a PWM signal to operate the SSR connected with the heating coil. Therefore, the algebraic transformation of current does not have a serious effect on the change of measurement noise distribution in transformed space.

4.2. First-Principles Model. In the present work, the heat transfer model of the preheating furnace has been developed on the basis of the principle of energy balances in the furnace media and the concept of one-dimensional convective heat transport phenomena.^{84,85} Figure 6 shows the schematic diagram of the preheating furnace. For the first principle model, the following assumptions have been considered:

1. The flow of air through the channel is an ideal plug flow; that is, there is an axial temperature gradient but no radial temperature gradient. The radial heat conduction through the tube wall is ideal and the axial heat conduction has been ignored.
2. The volume of the channel is constant; that is, the inlet flow and outlet flow are equal.
3. The physical properties of the system, such as density and specific heat, are constant.
4. Different heat transfer coefficients (α_x) are constant.
5. The dynamics on the coil side is ignored; that is, heat energy produced in the coil reacts instantaneously to changes in the supply current.
6. The coil temperature is not affected by the pipe or air temperature, as the coil is not in direct contact with the pipe.
7. The furnace wall is lumped in one section, though in reality different layers are arranged from inside to outside.
8. Heat and mass transfer is considered to take place mostly by forced convection.

4.2.1. Energy Balance Equations. For the preheater as shown in Figure 6, if $T_c(z)$, $T_p(z)$, and $T_a(z)$ are the temperature of coil, pipe, and air, respectively, at some point z , α_c and α_a are the heat transfer coefficient at the coil and airflow side, A_c and A_a are the heat transfer area per unit length at coil and airflow side, M_p and C_p are the mass of the pipe per

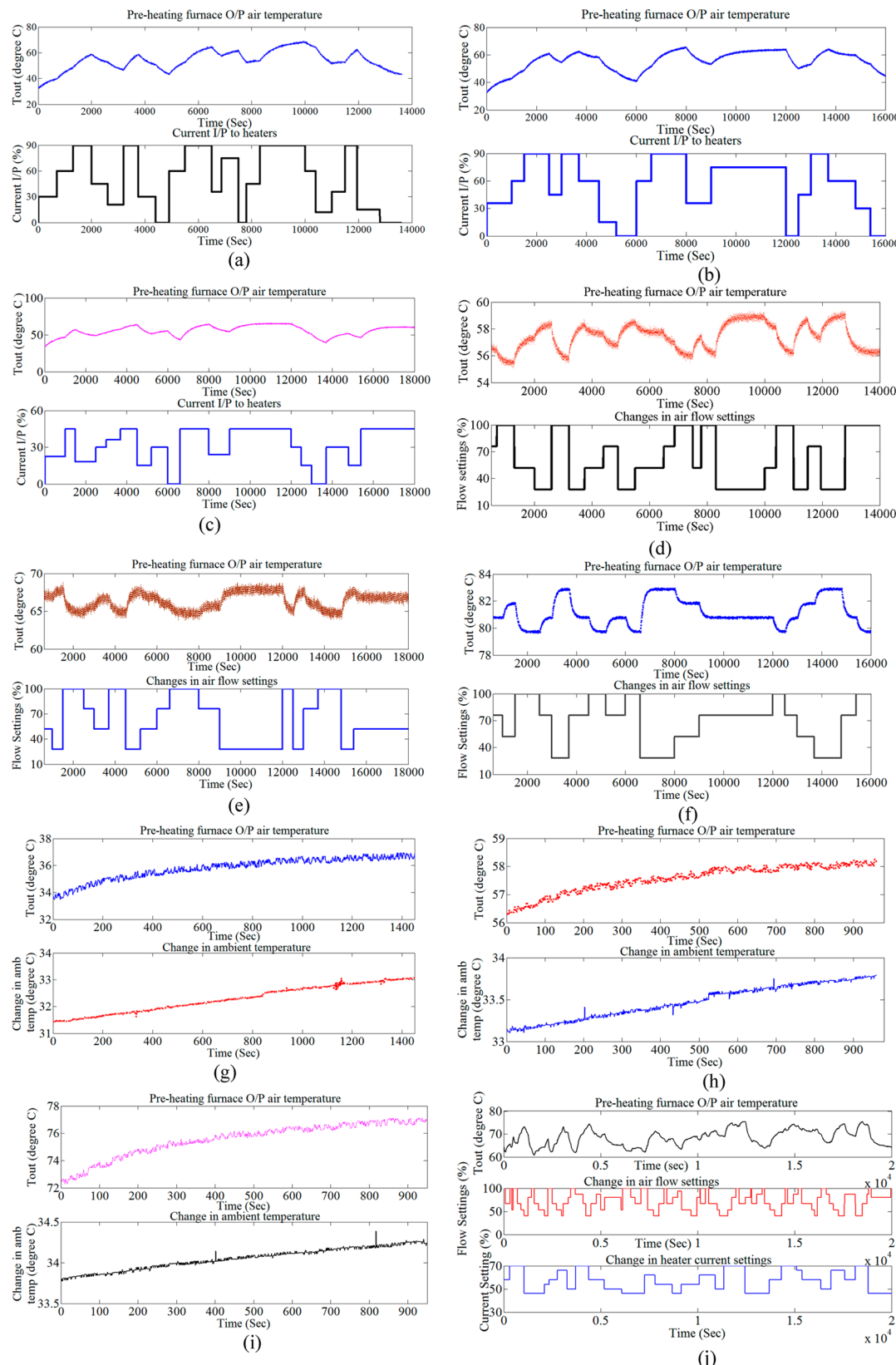


Figure 5. Input current settings and corresponding variations of outlet air temperature T_{out} ($^{\circ}\text{C}$) as obtained in mode-1, for the for the air flow rate in the (a) lower, (b) medium, and (c) higher regions. Input airflow rate settings and the corresponding variation of T_{out} ($^{\circ}\text{C}$) as obtained in mode-2, for the current settings of (d) lower, (e) medium, and (f) higher regions. Ambient temperature variations and the corresponding variation of T_{out} ($^{\circ}\text{C}$) as obtained in mode-3, in the (g) lower (current setting, 30%; flow setting, 100%) (h) medium (current setting, 60%; flow, setting 50%) and (i) higher (current setting, 90%; flow setting, 25%) regions. Variation of T_{out} ($^{\circ}\text{C}$) as obtained in mode-4, due corresponding changes in current, air flow rate (shown panel j).

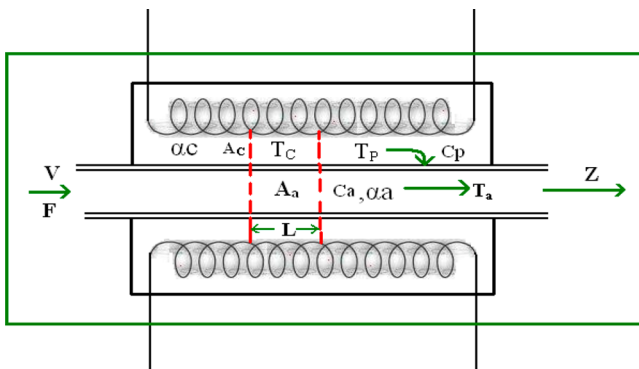


Figure 6. Schematic diagram of the preheater.

unit length and specific heat of the pipe, then the energy balance for a section of the wall at every point z can be written as

$$M_p C_p \frac{\delta T_p}{\delta t} = \alpha_c A_c (T_c - T_p) - \alpha_a A_a (T_p - T_a) \quad (19)$$

where $T_c(z)$, $T_p(z)$, and $T_a(z)$ are represented as T_c , T_p , and T_a .

The left-hand side term of 19 represents the accumulation of energy by the pipe, the first term at the right-hand side is the heat transfer from the coil to the pipe and the last term is the heat transfer from the pipe wall to the duct air.

Now, if the air has mass flow rate of F , with M_a and C_a being the mass of the air per unit length and specific heat of the air, then the energy balance of the fluid can be written as

$$M_a C_a \frac{\delta T_a}{\delta t} + F C_a \frac{\delta T_a}{\delta z} = \alpha_a A_a (T_p - T_a) \quad (20)$$

The first term is accumulation of energy by the air, the second term is the transportation of energy, and the third term is the supply of energy from pipe walls to air.

Similarly heat balance for the coil can be represented as

$$M_c C_c \frac{\delta T_c}{\delta t} = Q - \alpha_c A_c (T_c - T_p) \quad (21)$$

where the left-hand side of eq 21 is the accumulation of energy, the first term at the right-hand side is the heat transfer due to the flow of current through the coil, and the last term is the heat transfer from the coil to the pipe wall.

Equations 19 and 20 can be written as

$$\tau_{cp} \frac{\delta T_p}{\delta t} = (T_c - T_p) - \frac{\tau_{cp}}{\tau_{pa}} (T_p - T_a) \quad (22)$$

$$\tau_a \frac{\delta T_a}{\delta t} + V \tau_a \frac{\delta T_a}{\delta z} = (T_p - T_a) \quad (23)$$

where $\tau_{cp} = M_p C_p / (\alpha_c A_c)$, $\tau_a = M_a C_a / (\alpha_a A_a)$, and $\tau_{pa} = M_p C_p / (\alpha_a A_a)$.

4.2.2. Steady State Analysis. Under steady state conditions (putting “s” in the subscript of variables to represent the steady state value), the derivatives with respect to time will be equal to zero. Thus, the pipe and air temperature both vary along the length of the cylinder, but remain invariant with respect to change in time. On the other hand coil temperature is uniformly distributed over the coil (*i.e.*, $T_{cs}(z) = T_{cs}$). Considering one-dimensional heat flow along the length of the furnace under steady state, with the help of boundary conditions presented in Table 1 and the approximation as

Table 1. Boundary Conditions for One Dimensional Heat Flow

$z = 0$	$T_a = T_{ins}$
$z = L$	$T_a = T_{outs}$

stated in the assumptions, from eq 22 and eq 23, the expression of outlet air temperature and the pipe temperature distribution along the length of the cylinder can be represented as

$$T_{outs} = T_{cs} - (T_{cs} - T_{ins}) e^{-L/(v_s \tau_a)} \quad (24)$$

$$T_{ps} = T_{cs} - \frac{\alpha_a A_a}{(\alpha_c A_c + \alpha_a A_a)} (T_{cs} - T_{ins}) e^{-z/(v_s \tau_a)} \quad (25)$$

4.2.3. Dynamic Model Analysis. The dynamic behavior of the model for changes in outlet air temperature as a function of changes in the heat flow to the heating coil, inlet air temperature, and duct airflow rate are analyzed by assuming

$$T_p = T_{ps} + \Delta T_p; \quad T_a = T_{as} + \Delta T_a; \quad T_c = T_{cs} + \Delta T_c;$$

$$Q = Q_{ss} + \Delta Q \quad \text{and} \quad v = v_s + \Delta v$$

The perturbation of each variable with respect to their respective steady state values are considered, and then by putting the steady-state condition and taking both sides of the Laplace transform of eq 22, the change in pipe temperature can be represented by

$$\Delta T_p(s) = \frac{\Delta T_c(s) + \frac{\tau_{cp}}{\tau_{pa}} \Delta T_a(s)}{\frac{\tau_{cp}}{\tau_{pa}} s + \frac{\tau_{cp}}{\tau_{pa}} + 1} \quad (26)$$

A similar dynamic analysis of eq 23 results in

$$\begin{aligned} v_s \frac{\partial(\Delta T_a)}{\partial z} + \left(s + \frac{1}{\tau_a} \right) \Delta T_a(s) \\ = \frac{1}{\tau_a} \Delta T_p - \frac{1}{\tau_a} (T_{cs} - T_{inlet}) e^{-z/(v_0 \tau_a)} \frac{\Delta v(s)}{v_s} \end{aligned} \quad (27)$$

Putting the value of ΔT_p from eq 26 in eq 27 gives

$$\begin{aligned} \frac{\partial(\Delta T_a)}{\partial z} + \frac{1}{v_s} \left[s + \frac{1}{\tau_a} \left(\frac{\tau_{cp} \cdot s + 1}{\tau_{cp} \cdot s + \frac{\tau_{cp}}{\tau_{pa}} + 1} \right) \right] \Delta T_a(s) \\ = \frac{1}{\tau_a v_s} \frac{\Delta T_c(s)}{\tau_{cp} \cdot s + \frac{\tau_{cp}}{\tau_{pa}} + 1} - \frac{1}{v_0} \left\{ \frac{1}{\tau_a} \frac{(T_{in} - T_{cs})}{v_s} e^{-z/v_s \tau_a} \right\} \Delta v(s) \end{aligned} \quad (28)$$

Further the dynamic analysis of eq 21 yields,

$$\Delta T_c(s) = \frac{K_q}{1 + \tau_c s} \Delta Q(s) + \frac{1}{1 + \tau_c s} \Delta T_p(s),$$

$$\text{where } K_q = 1/\alpha_c A_c \quad (29)$$

Since electric heater or coils are placed inside the furnace and have no direct contact with the pipe, any change in pipe temperature does not make a significant change in the coil temperature. Therefore, the effect of pipe temperature on the coil temperature can be neglected. Therefore, eq 29 can be simplified as follows:

$$\Delta T_c(s) = \frac{K_q}{1 + \tau_c s} \Delta Q(s) \quad (30)$$

By finding the general and particular solutions by setting the boundary conditions as given in Table 1 and substituting $\Delta T_c(s)$ from eq 30, the solution of eq 28 at $z = L$ can be found as shown in eq 31.

$$\begin{aligned} \Delta T_{\text{out}}(s) &= \Delta T_a(L, s) \\ &= \frac{1}{(1 + \tau_c s) \left(1 + \left(\tau_a + \tau_{cp} + \frac{\tau_{cp}}{\tau_{pa}} \tau_a \right) s + \tau_a \tau_{cp} s^2 \right)} \\ &\left[1 - \exp \left(- \left(\tau_a s + \frac{\tau_{cp} s + 1}{\tau_{cp} s + \frac{\tau_{cp}}{\tau_{pa}} + 1} \right) \frac{L}{v_0 \tau_a} \right) \right] \Delta Q(s) \\ &- \left[\frac{1 + \frac{\tau_{cp}}{\tau_{pa}} + \tau_{cp} s}{1 + \left(\tau_a + \tau_{cp} + \frac{\tau_{cp}}{\tau_{pa}} \tau_a \right) s + \tau_a \tau_{cp} s^2} \frac{(T_{cs} - T_{\text{inlet}})}{v_0} \exp \left(\frac{(T_{cs} - T_{\text{inlet}})}{v_0} \right) \right. \\ &\left. - \frac{L}{v_0 \tau_a} \left(1 - \exp \left(- \left(\tau_a s + \frac{\tau_{cp} s + 1}{\tau_{cp} s + \frac{\tau_{cp}}{\tau_{pa}} + 1} \right) \frac{L}{v_0 \tau_a} \right) \right) \right] \Delta \nu(s) \\ &+ \exp \left(- \left(\tau_a s + \frac{\tau_{cp} s + 1}{\tau_{cp} s + \frac{\tau_{cp}}{\tau_{pa}} + 1} \right) \frac{L}{v_0 \tau_a} \right) \Delta T_{\text{in}}(s) \end{aligned} \quad (31)$$

In 31, each term in the right-hand side expression consists of an exponentially decaying function, that is,

$$\exp \left(- \left(\tau_a s + \frac{\tau_{cp} s + 1}{\tau_{cp} s + \frac{\tau_{cp}}{\tau_{pa}} + 1} \right) \frac{L}{v_0 \tau_a} \right) = e^{-h(s)z}$$

which gradually decreases along the length of the air preheating chamber. The $h(s) = (1/v_0 \tau_a) [\tau_a s + ((\tau_{cp} s + 1)/(\tau_{cp} s + (\tau_{cp}/\tau_{pa}) + 1))]$ basically represents the weighting function. The rise of instantaneous air temperature inside the chamber or at the outlet of the air preheating chamber is a function of changes in ambient, coil temperature, and air flow velocity, respectively, but how fast the air temperature would rise or fall is dependent on $h(s)$, irrespective of changes in the input conditions independently.

Since the heat transfer area per unit length at coil (A_c) and airflow (A_a) side are nearly equal [$A_c \triangleq A_a$] and the heat transfer coefficient at the coil (α_c) is much greater than the heat transfer coefficient at airflow side (α_a) [$\alpha_c \gg \alpha_a$], then

$$\frac{\alpha_a A_a}{\alpha_c A_c} \ll 1 \quad (32)$$

Equation 32 can be rewritten as

$$\frac{\alpha_a A_a / M_p C_p}{\alpha_c A_c / M_p C_p} \ll 1 \quad \text{i.e., } \frac{\tau_{cp}}{\tau_{pa}} \ll 1 \quad (33)$$

Now on the basis of eq 33, the function $h(s)$ can be approximated as follows:

$$h(s) = \frac{1}{v_s \tau_c} \left[\tau_a s + \frac{\tau_{cp} s + 1}{\tau_{cp} s + 1} \right] = \frac{1}{v_s \tau_c} [\tau_a s + 1] \quad (34)$$

Therefore, with the help of the approximation as stated in eq 34 and eq 30, the changes in outlet air temperature computed in eq 31 can be represented as eq 35:

$$\begin{aligned} \Delta T_{\text{out}}(s) &= \Delta T_a(L, s) \\ &= \frac{1}{(1 + \tau_c s)(1 + (\tau_a + \tau_{cp})s + \tau_a \tau_{cp} s^2)} \\ &\left[1 - \exp \left(- (\tau_a s + 1) \frac{L}{v_0 \tau_a} \right) \right] \Delta Q(s) \\ &- \left[\frac{1 + \tau_{cp} s}{1 + (\tau_a + \tau_{cp})s + \tau_a \tau_{cp} s^2} \frac{(T_{cs} - T_{\text{inlet}})}{v_0} \exp \left(- \frac{L}{v_0 \tau_a} \right) \right. \\ &\left. \left(1 - \exp \left(- (\tau_a s + 1) \frac{L}{v_0 \tau_a} \right) \right) \right] \Delta \nu(s) \\ &+ \exp \left(- (\tau_a s + 1) \frac{L}{v_0 \tau_a} \right) \Delta T_{\text{in}}(s) \end{aligned} \quad (35)$$

Again from eq 24, we have

$$\exp \left(- \frac{L}{v_s \tau_a} \right) = \frac{T_{cs} - T_{\text{outs}}}{T_{cs} - T_{\text{ins}}} \quad (36)$$

Now when eq 35 is substituted by eq 36, the expression of change in the chamber outlet air temperature can be represented by eq 37, where time constant $\tau_R = \tau_a \times \ln((T_{cs} - T_{\text{inlet}})/(T_{cs} - T_{\text{out}}))$.

$$\begin{aligned} \Delta T_{\text{out}}(s) &= \frac{T_{cs} - T_{\text{out}}}{T_{cs} - T_{\text{inlet}}} e^{-\tau_R s} \Delta T_{\text{in}}(s) \\ &+ \frac{1}{(1 + \tau_c s)(1 + (\tau_a + \tau_{cp})s + \tau_a \tau_{cp} s^2)} \\ &\left[1 - \frac{T_{cs} - T_{\text{out}}}{T_{cs} - T_{\text{inlet}}} e^{-\tau_R s} \right] \Delta Q(s) \\ &- \left[\frac{1 + \tau_{cp} s}{1 + (\tau_a + \tau_{cp})s + \tau_a \tau_{cp} s^2} \frac{(T_{cs} - T_{\text{inlet}})}{v_0} \right. \\ &\left. \left(1 - \frac{T_{cs} - T_{\text{out}}}{T_{cs} - T_{\text{inlet}}} e^{-\tau_R s} \right) \right] \Delta \nu(s) \end{aligned} \quad (37)$$

In the present modeling framework a linear time invariant (LTI) system has been considered, where preheating the chamber outlet temperature is a superposition of the outputs of three models (model I, II, and III). In the formulated LTI system, each model represents a separate subsystem. The output of the subsystems derived from first-principles interacts with the changes in heat input, airflow rate, and ambient temperature, respectively, in an independent manner. Thus,

$$\Delta T_{\text{out}} = \frac{\partial T_{\text{out}}}{\partial Q} \Delta Q + \frac{\partial T_{\text{out}}}{\partial \nu} \Delta \nu + \frac{\partial T_{\text{out}}}{\partial T_{\text{in}}} \Delta T_{\text{in}} \quad (38)$$

The comparison of eq 37 with eq 38 results in

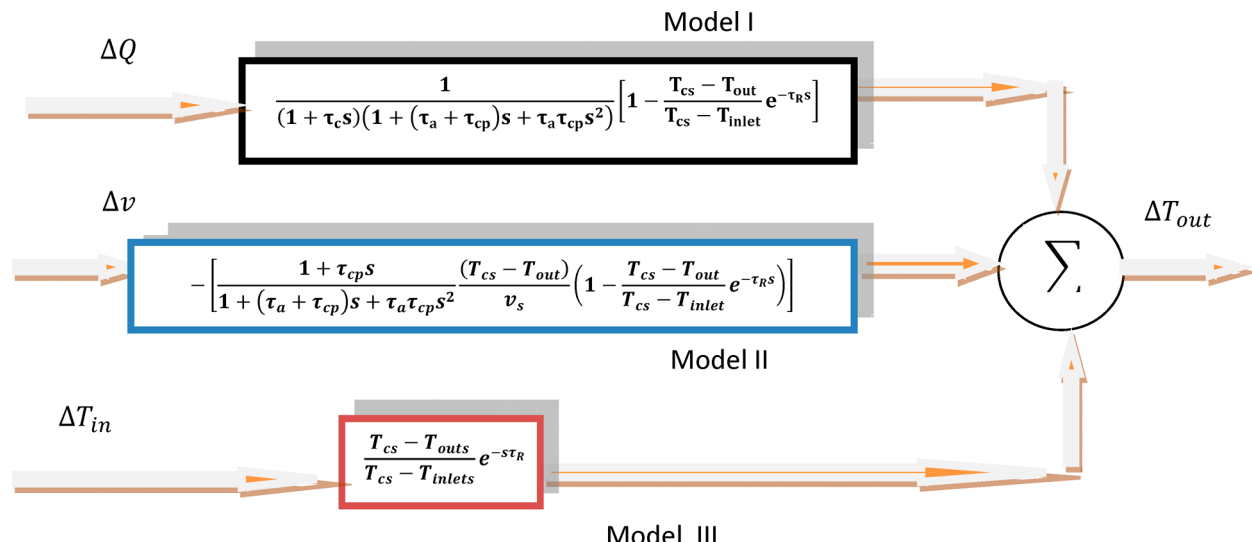


Figure 7. Block diagram representation of the process.

Model I:

$$\frac{\Delta T_{out}}{\Delta Q} = \frac{1}{(1 + \tau_c s)(1 + (\tau_a + \tau_{cp})s + \tau_a \tau_{cp} s^2)} \left[1 - \frac{T_{cs} - T_{out}}{T_{cs} - T_{inlet}} e^{-\tau_R s} \right] \quad (39)$$

Model II:

$$\frac{\Delta T_{out}}{\Delta v} = -\left[\frac{1 + \tau_{cp} s}{1 + (\tau_a + \tau_{cp})s + \tau_a \tau_{cp} s^2} \frac{(T_{cs} - T_{out})}{v_s} \left(1 - \frac{T_{cs} - T_{out}}{T_{cs} - T_{inlet}} e^{-\tau_R s} \right) \right] \quad (40)$$

Model III:

$$\frac{\Delta T_{out}}{\Delta T_{in}} = \frac{T_{cs} - T_{outs}}{T_{cs} - T_{inlets}} e^{-s\tau_R} \quad (41)$$

It is to be noted here, though there are some common parameters like τ_R , τ_a , and τ_{cp} among the three different models, the parameter values will be different for the three models depending upon the operating conditions.

The overall thermal model of the air preheating furnace can be developed from 39, 40, and 41. The block diagram representation of the thermal model is shown in Figure 7.

4.3. Model Estimation and Validation. The system identification certainly requires a fixed model structure prior to identification of the model parameters. But it is not convenient to obtain the model parameters directly from experimental data collections, particularly using the set of mathematical models as described by eq 39 and eq 40 [model I and II], because the models contain a delayed and an undelayed part along with the same third/second order lag transfer function, respectively. Therefore, to handle such a problem, for each model initially the time delay between the input and output signal was estimated and then the delayed and an undelayed part of the input was treated as two separate inputs, and consequently these strategies resulted in the good fit of the models.

There is significant research work contributing to the system identification in both the “discrete time (DT)” or “continuous time (CT)” frameworks. Continuous-time identification is preferred when the input and output signals are CT functions but sampled at discrete time instants. Because of the physical meaning of the identified parameters in a conventional manner, a continuous-time (CT) model was considered in this work. A continuous-time (CT) domain model may be identified through indirect and direct approaches. In the “direct” approach, the CT model is identified directly from DT data.⁸⁶ A number of algorithms belong to the conventional system identification techniques. Among these the prediction errors (PE) method and the instrument variable (IV) method are quite popular for both simulated and real data. The methods for CT model identification have been applied in various forms such as state vector filtering (SVF), instrumental-variable (IV), generalized Poisson moment functional (GPMF), subspace state-space estimation (N4SID), and simplified refined instrumental variable method for continuous-time (SRIVC).^{86,87,91–94} The merits and demerits of these methods have been studied in detail by Ljung et al.⁸⁶ In the present work for identifying the data driven models, various CT model identification algorithms like SRIVC, SVF, IV, GPFM, and N4SID of CONTSID toolbox^{88,89} and SYSID toolbox of MATLAB⁹⁰ have been used.

In the present contribution of model identification, all these methods have been studied so that the best method for the present application can be obtained. To compare the performances, the highest value of coefficient-of-determination (R_T^2), which is a statistical measure has been considered. The R_T^2 has been calculated using eq 42; the details can be found in ref :

$$R_T^2 = \left(1 - \frac{\|y - y_s\|_2^2}{\|y - \bar{y}\|_2^2} \right) \quad (42)$$

The y denotes measured output, y_s denotes simulated output, and \bar{y} is the mean of y . R_T^2 indicates how well the model output fit to the plant output and must be close to 1. The statistical attribute R_T^2 alone may not be sufficient to avoid over parametrization and to identify a parsimonious model,⁸⁷ therefore another popular statistical attribute, that is, Young's

information criterion (YIC) has been used before selecting the model order.⁸⁷ The statistical measure YIC provides information about the overparametrization in the selected models, and a greater negative value of the YIC ensures a better model fit.

For construction and validation of the model the experimental data sets as collected during the series of experiments have been utilized. Among the three sets of data for each of the conditions, one randomly chosen set has been kept entirely separate for final testing of the proposed technique. The remaining two data sets have been used for training and validation using a 2-fold cross-validation (cv) test. In the 2-fold cv technique one data set is used for training, and the remaining one is used for testing. In the next cycle, the previously used test data set is used in training and the previous training set is used in testing. In this way after completion of two cycles the average values of the performance parameters, that is, R_T^2 and YIC are calculated and presented for analysis. This method has been followed in both stages, that is, for the determination of model order and also for determination of model parameters. After searching the best set of model structures along with the parameter values, all three models were finally tested with the fresh set of data; the test results are discussed in the following section.

4.4. Process Nonlinearities. The process under investigation accommodates saturation nonlinearity, encountered due to the presence of actuator saturation. Depending upon the percentage output setting of the controller, the final control element solid-state relay (SSR) exhibits saturation nonlinearity. For instance, if the controller percentage output setting is <10% and >90%, then the average current output of the final control element (SSR) gets saturated. Here the manipulated variable ΔQ was computed by squaring the changes in measured current data. The error involved in the measurement of current, was significantly low as it was estimated from the TPO-duty cycle of PLC, which generates a PWM signal to operate the SSR connected with the heating coil. Therefore, the algebraic transformation of current does not have a serious effect in the change of measurement noise distribution in the transforming space. Therefore, the changes in heat input ΔQ can easily be computed from the transfer characteristic of ΔQ and ΔI .

5. CONTROL DESIGN

This section discusses about the objective function formulation for developing automatic loop shaping algorithm and refined PSO enabled automated QFT (Refined PSO-QFT) algorithm.

5.1. Formulation of Constraints and Objective Functions for Automatic Loop Shaping in QFT. In the proposed approach the controller structure is predetermined and is given by^{55,79,80}

$$C(s) = \frac{b_r s^r + \dots + b_1 s + b_0}{a_n s^m + \dots + a_1 s + a_0} \quad (43)$$

The problem of the loop-shaping QFT environment can be facilitated to a multi-objective linear constraint optimization problem. The objective function is formulated by taking the linear weighted sum of various constraints involved with the loop-shaping problems in QFT. In the present framework as per the requirement of the control problem the objective function J is defined by considering the following three indices. (a) Constraint/index for high frequency gain (J_{hfg}): The restriction on high frequency gain of the controller is

considered to minimize the control effort. (b) Index for robust stability, performance, and disturbance rejection bounds (composite of all bounds) (J_b): In the QFT design, various low and high frequency bounds are computed for all design frequencies using the available plant templates and stability, performance, and disturbance rejection specifications. The composite of all bounds impose a certain restriction in shaping nominal loop transfer functions. The synthesized nominal loop must satisfy its corresponding bound value at all design frequencies. (c) Index for stability of nominal loop transmission function (J_{sta}): It deals with roots or pole locations of the nominal loop transmission function $L_0(j\omega)$.

Therefore, the objective function is given by

$$J = \mu_1(t) J_{\text{hfg}} + \sum_{i=1}^N [\mu_{2i}(t) J_{\text{sta}i} + \mu_{3i}(t) J_{\text{bi}i}] \quad (44)$$

where, J_{bi} and $J_{\text{sta}i}$ are the bound and stability indices at the i th design frequency, respectively, and N indicates the number of discrete points taken as designed frequencies. $\mu_1(t)$, $\mu_2(t)$, and $\mu_3(t)$ are the weighting factors for t th iteration. As suggested by the various literature of developing an automatic loop-shaping algorithm using population-based search techniques, most of the researchers considered death penalties in defining the objective functions. But the death penalty function certainly suffers from some disadvantages. Deciding on an optimal (or near-optimal) value of the weight is a difficult optimization problem itself: (i) If the weight is too small, an infeasible solution may not be penalized enough. Hence, infeasible solutions may be evolved by the search method. (ii) If the weight is too large, a feasible solution is very likely to be found, but could be of very poor quality. A large value of weight discourages the exploration of infeasible regions.

Therefore, to minimize the probability of finding infeasible and poor quality solutions in the search space, some adaptive modifications have been considered in selecting the weight of penalty functions. In this method, penalty parameters $\mu: [\mu_{11}, \mu_{12}, \dots, \mu_{1N}, \mu_{21}, \mu_{22}, \dots, \mu_{2N}] e \mathbb{R}^{2N+1}$ are updated for every q iteration according to information gathered from the population.⁹⁵

The j th penalty function μ_j is updated in every q iterations as follows:

$$\mu_j(t+1) = \begin{cases} \left(\frac{1}{\Gamma_1}\right)\mu_j(t) & \text{if all the best particle in the last } q \\ & \text{iterations are feasible} \\ \Gamma_2\mu_j(t) & \text{if they are not feasible} \\ \mu_j(t) & \text{otherwise} \end{cases} \quad (45)$$

It indicates, if all best particles of last q iterations are feasible, penalty term $\mu_j(t+1)$ for iteration $(t+1)$ decreases. If they are unfeasible, the penalty term is increased. Otherwise if the best individuals in the last q iterations consist of feasible and unfeasible solutions, the penalty term does not change. Γ_1 and Γ_2 are the scaling factors and $\Gamma_1, \Gamma_2 > 1$, $\Gamma_1 > \Gamma_2$, and $\Gamma_1 \neq \Gamma_2$.

For an automated design, the stability is analyzed by checking the roots of the characteristics equation of the compensated nominal loop ($L_0(j\omega)$). A simple cost function to penalize an unstable design is

$$J_{\text{sta}} = \begin{cases} 0 & \text{if stable} \\ 1 & \text{if unstable} \end{cases} \quad (46)$$

To obtain the cost function J_{bi} for QFT bound indices at all designed frequencies, initially it is required to generate robust stability, performance and disturbance rejection bounds for the given design specifications and amount of plant uncertainties by using the QFT tool box. Then intersections between the different bounds are taken for all design frequencies. Thus, the compound bounds are generated. Then, with the capability and flexibility of an evolutionary algorithm, these numerical bounds can be used directly in an automated design. At each frequency point, the gain and phase of the open loop transmission $L(j\omega_i)$ is calculated and then checked to see whether or not the QFT bound at all designed frequencies are satisfied. A simple QFT bound index is given by

$$J_{bi} = \begin{cases} 0 & \text{if QFT bound at } \omega_i \text{ is satisfied} \\ d_{bi} & \text{otherwise} \end{cases} \quad (47)$$

where d_{bi} is the distance to the QFT bound at i th frequency point. Since the nominal plant is fixed, the cost function for high frequency gain is calculated from the high frequency gain of the controller given by

$$J_{\text{hfg}} = b_r/a_m \quad (48)$$

The coefficients b_r, \dots, b_1, b_0 , and a_m, \dots, a_1, a_0 are searched by the PSO algorithm to satisfy the constant equations. a_m can be set to 1.

5.2. Refined PSO Enabled Automated QFT (Refined PSO-QFT) Algorithm. The Refined PSO-QFT algorithm integrates QFT, PSO, and adaptive penalty functions. The modified algorithm involves the following steps:

Step 1: Define the process model, uncertainties, robust stability, tracking performance, and plant input/output disturbance rejection specifications.

Step 2: Obtain the upper and lower tracking models from robust tracking performance specifications and select the design frequencies from tracking models.

Step 3: Define nominal plant and generate plant templates at all design frequencies.

Step 4: Compute the bounds for the respective design specification using eq 1, 6–15 and check to see whether the solution exists. If exists goto next step, else back to **Step 1** and modify the corresponding design specification.

Step 5: Compute the composite bounds for all design frequencies.

Step 6: Select the controller order “ m ” and define the controller structure.

Step 7: Construct the nominal loop transmission function $L_0(j\omega)$ using eq 4.

Step 8: Initialize a population of g particles with random positions within the lower and upper bound of the problem space. Similarly initialize randomly g velocities associated with the particles. Also specify the maximum number of iteration and fitness error limit.

Step 9: Initialize the initial weight of the penalty functions in 44 and scaling factor Γ_1 and Γ_2 . Select the weights suitably, that is, $\mu_1(0) > \mu_2(0) > \mu_3(0)$ and $\Gamma_1, \Gamma_2 > 1$, $\Gamma_1 > \Gamma_2$, $\Gamma_1 \neq \Gamma_2$. Also set the value of generation q .

Step 10: Evaluate the optimization fitness functions J for the initial population using eq 44.

Step 11: Find the minimum fitness value for fitness functions J in **Step 10** and call it J_{pbest} and let the particle associated with it be X_p .

Step 12: Initially set J_{gbest} equal to J_{pbest} .

Step 13: Update the weight Q using eq 18.

Step 14: Update the velocity of each particle using eq 16.

Step 15: Check V for the range $[V_{\text{max}}, V_{\text{min}}]$. If not, set it to the limiting values.

Step 16: Update the position of each particle using eq 17, which gives the new population.

Step 17: Evaluate $C(j\omega)$ and $L_0(j\omega)$ for the new population using eq 43 and eq 4.

Step 18: Repeat **Step 15** for the new population.

Step 19: Evaluate the optimization fitness functions J for new population.

Step 20: Obtain new J_{pbest} for fitness functions J for new population.

Step 21: Compare the J_{pbest} obtained in step 20 with J_{gbest} . If J_{pbest} is better than J_{gbest} then set J_{gbest} to J_{pbest} .

Step 22: Check the convergence criteria (maximum number of iteration, fitness value). If met goto **Step 26** else goto **Step 13** and update iteration count by one.

Step 23: Check the iteration count. If iteration count = q check the fitness values of J_{pbest} for the last q iterations, else goto **Step 14**.

Step 24: if all best particles of last q iterations are feasible, update the penalty by $(1/\Gamma_1)\mu(\text{iter})$, else if no feasible fitness value update the penalty by $\Gamma_2\mu(t)$, else do not update the penalty.

Step 25: Modify the objective function J and goto **Step 14**.

Step 26: Synthesize the nominal loop on Nichols chart using optimized values of controller parameter.

Step 27: Synthesize the prefilter.

Step 28: Validate the results in both the time and frequency domains.

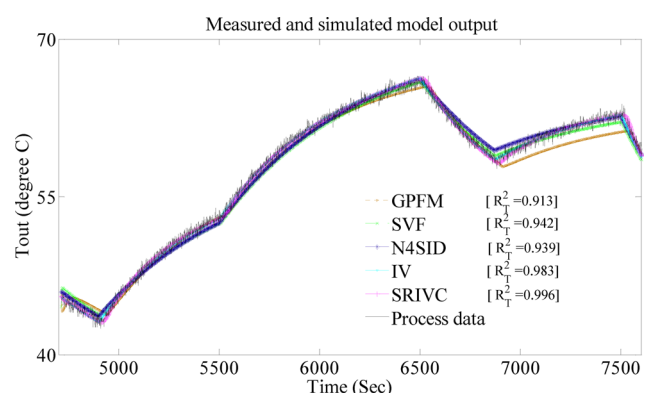
6. RESULTS AND DISCUSSION

The obtained results, grouped in six categories are presented in the following subsections. These are the continuous domain identification method selection, control oriented model estimation, model validation, control design using refined PSO-QFT method, and finally validation and discussion.

6.1. Identification Method Selection. To select the identification method various continuous domain (CT) methods like state vector filtering (SVF), instrumental-variable (IV), generalized Poisson moment functional (GPMF), subspace state-space estimation (N4SID) and simplified refined instrumental variable method for continuous-time (SRIVC) have been studied, and different statistical attributes like coefficient-of-determination (R^2_T) and Young's information criterion (YIC) were computed using the identification data sets collected under three different operating modes (presented in Table 2) for the model structures as specified in eq 39, 40, and 41. From the initial experiments it was observed that the performance of SRIVC was best and consistent among the different algorithms. As an illustration, comparisons between the different methods for a section of the experimental data set collected under mode-1 with a fixed flow setting in the lower range is shown in Figure 8. It was observed that the SRIVC methods performed best in all the cases, when compared to other algorithms. Therefore, in this work SRIVC has been studied in detail with different initialization techniques such as least-squares SVF (LSSVF), instrumental-variable generalized

Table 2. Statistical Attributes for Different Models with Various Identification Methods

SYSID Method	Statistical Attributes	
	R_T^2	YIC
Model I		
GPFM	0.913	-5.238
SVF	0.942	-7.321
N4SID	0.939	-9.51
IV	0.983	-10.76
SRIVC	0.996	-11.87
Model II		
GPFM	0.952	2.667
SVF	0.946	-5.83
N4SID	0.977	-9.47
IV	0.992	-11.87
SRIVC	0.998	-14.76
Model III		
GPFM	0.884	-2.391
SVF	0.887	-5.49
N4SID	0.912	-7.42
IV	0.921	-8.42
SRIVC	0.926	-8.36

**Figure 8.** Comparisons between different methods (SRVC, GPMF, SVC, N4SID, and IV) based on the value of R_T^2 for the data set collected under mode-1 for a current setting in the lower range.

Poisson moment functional (IVGPMF), and simplified refined instrumental variable (SRIV) algorithm. It was further observed that SRIVC initiated by different routines like LSSVF, IVGPMF, and SRIV performed in a similar fashion and resulted in similar performance except for few cases. Especially for the SRIVC algorithm initiated by IVGPMF some inconsistent results were reported because of a mismatch of the cutoff frequency of the Poisson filter chain element required for the initial parameter estimation by the IVGPMF routine.

SRIVC is one of the model predictive approaches and belongs to the IV method. The key idea of SRIVC identification is to assume that the disturbing noise is only available at the sampling instances, and termed as filtered discrete white noise. An iterative SRIVC is a successful stochastic identification technique^{86–94} also reported by various researchers; present results also reaffirm those findings.

This approach involves a method of adaptive prefiltering based on a quasi-optimal statistical solution to the problem when the additive noise is white. This technique has the advantage of not requiring manual specification of prefilter parameters. The method is based on the maximum likelihood

(ML) approach in which the error function is defined by the output error (OE) and minimized by the least-squares criterion.

6.2. Estimation of Model Parameters. Finally the parameters of the three different models (Figure 7) were identified as per desired structure obtained using the SRIVC method under LSSVF initialization. The 2-fold cv technique as discussed earlier was used to find the best set of parameter values, for each of the models. To identify model I and model II as per the desired structure, the time delay between input and output signals were estimated initially from the experimental data sets collected under operating mode 1 and 2, and the time delays were found to be 13 and 4 samples, respectively. While the data sets were collected, the loop rate of DCS was set to 1 Hz, that is, various data sets were recorded in one second intervals. Therefore, for model I and model II the time delay was obtained as 12 and 4 s, respectively. Then the model estimations were carried out by using the SRIVC method by following the procedure as discussed in section 4.3. To identify the parameters of model III, a first order Pade approximation⁹⁶ was taken to shape the model into identifiable form. The identified control oriented models and their respective parametric uncertainty regions are presented in Table 3. The identified models were found to be highly uncertain due to parametric variations at different operating regions. Therefore, robust parametric control may be a reasonably suitable choice.

6.3. Model Validation and Discussion. After the estimation of best suitable model parameters for each of the three models, further test has been performed in different operating regions for the respective models with an independent testing data set, as discussed earlier. Further model validation study was carried out in the complete *multi-input-single-output* model with the data set collected in mode-4. During the complete model validation study the nominal plants for the three models were considered.

Plots of experimental data and corresponding model response with the different portions of excitation as presented in Figure 5 is presented in Figure 9 panels a–c. Figure 9a shows the comparison for the portion of the experimental data (as presented in Figure 5b) with model I, Figure 9b shows the comparison of the model II for the portion of the experimental data as shown in Figure 5f, and Figure 9c shows the similar comparison for the model III, when the room air conditioning was switched off and other inputs were set to respective medium values (experimental data as shown in Figure 5h). Figure 9d shows the complete nominal plant response when all the inputs are varied simultaneously; the corresponding portions of the signals are presented in Figure 5j. It is evident from Figure 9 panels a–c that the responses of the identified models are closely correlated with the respective response of the actual process when various inputs are applied separately. Since the simulated response was found to be reasonably close to the experimental response, it can be claimed that the approximations considered for simplification to find a suitable lower order model are appropriate for control design and implementation.

From Figure 9d, it can be observed that the response of the nominal plant model (one selected plant model from the family of uncertain plant models) is quite capable of following the trends of experimental data. The response of the nominal plant and the actual process are almost indistinguishable in the middle region (i.e. flow and current setting both are in middle range), but there are some deviations in the lower and higher region of operation. This is because of the parameters of the

Table 3. Control Oriented Models^a

input	identified model parameters	parametric uncertainty in regional model (model inaccuracy) (abs value)	range of parametric variation for the overall model (min and max value with % variation)
Model I			
lower	$\beta_{11} = 1.1919 \times 10^{-9}, k_1 = 0.3177, \alpha_{12} = 0.0024,$ $\alpha_{11} = 2.3595 \times 10^{-5}, \alpha_{10} = 2.2845 \times 10^{-8}$	$\beta_{11}: \pm 4.546 \times 10^{-10}, \alpha_{12}: \pm 0.001675, \alpha_{11}: \pm 9.043 \times 10^{-6}, \alpha_{10}: \pm 1.51 \times 10^{-8}$	$\beta_{11} \in [7.3730 \times 10^{-10}, 2.0099 \times 10^{-7}], \pm 49.81\%$
medium	$\beta_{11} = 1.0477 \times 10^{-7}, k_1 = 7.1538 \times 10^{-4}, \alpha_{12} = 0.0083,$ $\alpha_{11} = 1.5024 \times 10^{-4}, \alpha_{10} = 2.5150 \times 10^{-7}$	$\beta_{11}: \pm 1.748 \times 10^{-9}, \alpha_{12}: \pm 0.001397, \alpha_{11}: \pm 3.126 \times 10^{-6}, \alpha_{10}: \pm 5.101 \times 10^{-9}$	$k_1 \in [3.2904e-04, 0.3177], \pm 49.95\%$
higher	$\beta_{11} = 1.9807 \times 10^{-7}, k_1 = 3.2904 \times 10^{-4}, \alpha_{12} = 0.0045,$ $\alpha_{11} = 3.1458 \times 10^{-4}, \alpha_{10} = 3.9748 \times 10^{-7}$	$\beta_{11}: \pm 2.923 \times 10^{-9}, \alpha_{12}: \pm 0.0004901, \alpha_{11}: \pm 6.445 \times 10^{-6}, \alpha_{10}: \pm 6.534 \times 10^{-9}$	$\alpha_{12} \in [7.2500 \times 10^{-4}, 0.0097], \pm 46.27\%$ $\alpha_{11} \in [1.4552 \times 10^{-5}, 3.2103 \times 10^{-4}], \pm 47.73\%$ $\alpha_{10} \in [0.2076 \times 10^{-8}, 3.7945 \times 10^{-8}], \pm 47.27\%$
Model II			
lower	$\beta_{21} = 0.4887, \beta_{20} = 0.2470, k_2 = 0.5433, \alpha_{21} = 4.4680,$ $\alpha_{20} = 0.0915$	$\beta_{21}: \pm 0.9101, \beta_{20}: \pm 0.4495, \alpha_{21}: \pm 8.101, \alpha_{20}: \pm 0.08312$	$\beta_{21} \in [0.0172, 0.8028], \pm 48.93\%$
medium	$\beta_{21} = 0.5191, \beta_{20} = 0.3174, k_2 = 0.4336, \alpha_{21} = 48.505, \alpha_{20} = 0.3695$	$\beta_{21}: \pm 0.2837, \beta_{20}: \pm 0.1373, \alpha_{21}: \pm 11.92, \alpha_{20}: \pm 0.1281$	$k_2 \in [3.2904e-04, 0.3177], \pm 24.46\%$
higher	$\beta_{21} = 0.0265, \beta_{20} = 0.0175, k_2 = 0.8490, \alpha_{21} = 1.4389,$ $\alpha_{20} = 0.0111$	$\beta_{21}: \pm 0.009347, \beta_{20}: \pm 0.01501, \alpha_{21}: \pm 1.298, \alpha_{20}: \pm 0.009$	$\beta_{20} \in [0.0025, 0.4547], \pm 49.73\%$ $\alpha_{21} \in [0.1409, 60.425], \pm 62.14\%$ $\alpha_{20} \in [0.0021, 0.4976], \pm 49.79\%$
Model III			
lower	$\beta_{31} = 0.03032, \beta_{30} = 0.000937, \text{ and } \alpha_{30} = 0.001968$	$\beta_{31}: \pm 0.002086, \beta_{30}: \pm 2.74 \times 10^{-5}, \text{ and } \alpha_{30}: \pm 5.32 \times 10^{-4}$	$\beta_{31} \in [0.0171, 0.0419], \pm 29.59\%$
medium	$\beta_{31} = 0.0192, \beta_{30} = 5.8190 \times 10^{-4}, \text{ and } \alpha_{30} = 0.0014$	$\beta_{31}: \pm 2.13 \times 10^{-3}, \beta_{30}: \pm 8.68 \times 10^{-5}, \text{ and } \alpha_{30}: \pm 0.000925$	$\beta_{30} \in [4.9510 \times 10^{-4}, 0.001], \pm 25.27\%$
higher	$\beta_{31} = 0.03518, \beta_{30} = 0.001005, \alpha_{30} = 0.002894$	$\beta_{31}: \pm 0.00673, \beta_{30}: \pm 3.42 \times 10^{-5}, \text{ and } \alpha_{30}: \pm 0.000342$	$\alpha_{30} \in [0.0014, 0.0032], \pm 28.12\%$

^aModel I

$$\frac{\Delta T_{\text{out}}}{\Delta Q} = \frac{\beta_{11}}{s^3 + \alpha_{12}s^2 + \alpha_{11}s + \alpha_{10}} [1 - k_1 e^{-13s}]$$

Model II

$$\frac{\Delta T_{\text{out}}}{\Delta v} = -\frac{\beta_{21}s + \beta_{20}}{s^2 + \alpha_{21}s + \alpha_{20}} [1 - k_2 e^{-4s}]$$

Model III

$$\frac{\Delta T_{\text{out}}}{\Delta T_{\text{in}}} = k_2 e^{-\tau_R s} = \frac{-\beta_{31}s + \beta_{30}}{s + \alpha_{30}}$$

nominal plant were selected from the average value of respective maximum and minimum parametric variations, so that the nominal plants selected from the set of uncertain plants for three different models are well suited for the middle region of operation.

Further, to justify the accuracy of identified models, different statistical indicators like *root-mean-square* error (RMS) and cross-correlation coefficient between measured and simulated response for the fresh data set were computed and found to be reasonably accurate. These values are presented in Table S1 (Supporting Information). The table also shows the performance measurements for the nominal, best, and worst case plant uncertainty with the data set collected under mode I. It was also observed that the data sets collected from the three sets of repeated tests at the same operating condition are not the same. There are some variations, which may be due to the presence of other uncertainties such as supply voltage variation, component drift, inaccuracies in measuring instruments, etc. The average of the rms errors and cross-correlation values of the repeated test data sets under different operating conditions were found to be 0.045 and 0.98, respectively.

The performance measures of the regionwise plants of the three models (i.e., models I, II, and III) are reasonably good,

and closer to the intradata set variations due to noises, therefore it validates the overall identification process.

The identification results also address that the process under consideration has large parametric variations due to the changes in operating regions and environmental conditions. Though it is generally agreed that the temperature response of the electrical heating furnace involving the pneumatic drying and conveying is much slower (for the process under investigation the average response time constant is 460–650 s⁸⁵) than the gas or oil fired furnace, a proper design and implementation of robust current and flow control strategies with prior knowledge of process models may reduce drying time and increase the overall efficiency of the drying process. This is studied in the following section.

6.4. Control Design. Consider the model I as presented in Table 3. Certainly the parameters of the model will vary widely depending upon the operating regions. Here the control design is carried out to find an appropriate robust current law for model I using a refined PSO-QFT method, where the effect of air flow settings on outlet air temperature has been considered as the plant output disturbances. The block diagram representation of the QFT closed loop control system is

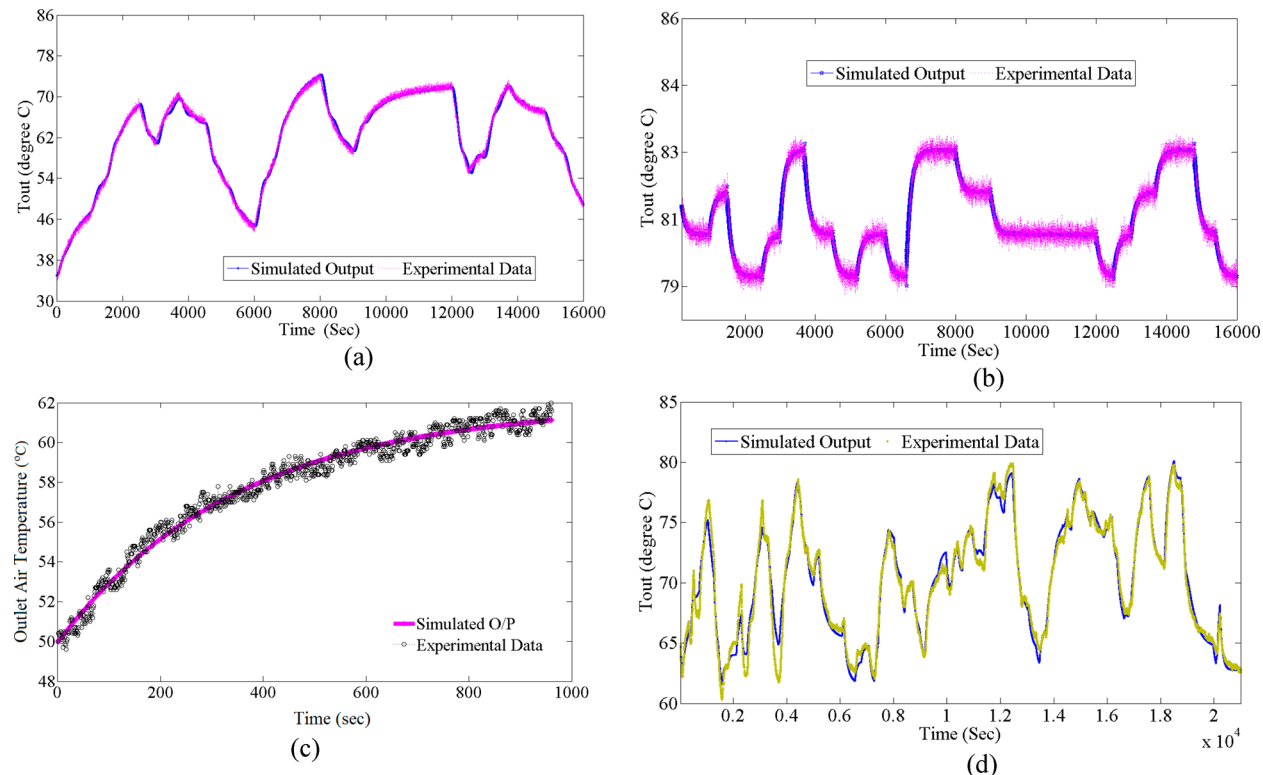


Figure 9. Comparison between simulated model response and respective fresh set of experimental data (a) mode I with airflow in the medium range, (b) mode II with current setting in the higher range, (c) mode III with current settings in the medium range, and (d) mode-IV and nominal plant response.

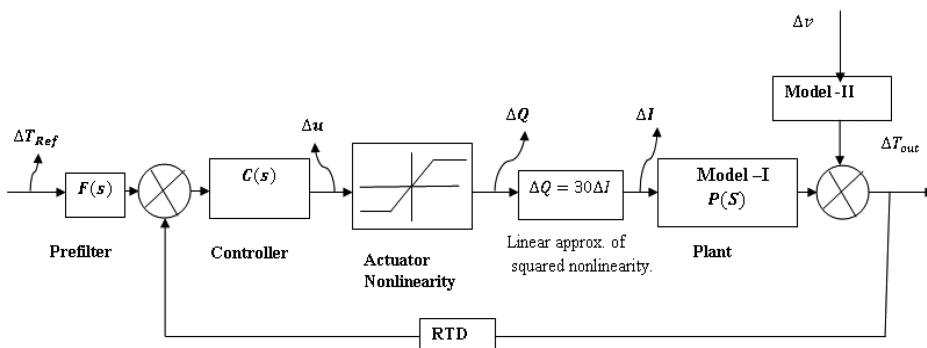


Figure 10. Block diagram representation of the QFT closed loop control system.

shown in Figure 10. The design intended to meet the following control objectives:^{48,49}

(1) Robust stability specification: The associated QFT robustness constraint in terms of the nominal loop transfer function, $L_0(j\omega) = P_0(j\omega)C(j\omega)$, is given by

$$\frac{\Delta T_{out}}{\Delta T_{ref}} = \left| \frac{L(j\omega)}{1 + L(j\omega)} \right| \leq \mu = 1.3 \quad (49)$$

which implies an approximately 4.95 dB gain margin and 45.12 degree phase margin for the closed loop system.

(2) Plant output disturbance rejection specification is considered from the worst case uncertain plant of model II, and given by

$$\frac{\Delta T_{out}(\omega)}{\Delta v(\omega)} \leq - \left| \frac{10.56(j\omega)^2 + 0.6905j\omega + 0.008066}{(j\omega)^3 + 104.3(j\omega)^2 + 3.007j\omega + 0.0127} \right| \quad (50)$$

(3) As per the requirement of the drying process and considering the actuator nonlinearities, the tracking performance specifications are chosen as

$$50 \leq \text{rise time}(t_r) \leq 200 \text{ sec}, \\ \text{no offset and overshoot} < 2\% \quad (51)$$

The nominal plant $P_0(s)$ is selected in the middle region the plant uncertainty of model I. The parameters of the nominal plant were selected from the average value of respective maximum and minimum parametric variations.

The nominal plant $P_0(s)$ is given by

$$P_0(s) = \frac{1.0086 \times 10^{-07}}{s^3 + 0.0052s^2 + 1.6779 \times 10^{-04}s + 2.0010 \times 10^{-08}} \\ \times [1 - 0.3180 \times 10^{-13}s] \quad (52)$$

Design frequencies are selected as

$$\omega = [0.001, 0.01, 0.05, 0.07, 0.15, 0.3, 0.5, 1, 15] \quad (53)$$

For automatic controller synthesis in MPSO-AQFT, a second-order controller is tentatively chosen as

$$C(s) = \frac{a_1 s + a_0}{s^2 + b_1 s + b_0} \quad (54)$$

Therefore, the compensated nominal loop $L(s)$ is given by

$$L(s) = P_0(s)C(s) \\ = \frac{1.0086 \times 10^{-7}}{s^3 + 0.0052s^2 + 1.6779 \times 10^{-4}s + 2.0010 \times 10^{-8}} \\ \times [1 - 0.3180 \times 10^{-13}s] \frac{a_1 s + a_0}{s^2 + b_1 s + b_0} \quad (55)$$

To permit optimization, all the coefficients of the chosen controller are allowed to vary in the four dimensional search spaces. During the optimization process the upper and lower bound of the coefficients within which each parameter can vary are given in Table S2 (Supporting Information). From the design specifications, eq 49 to eq 51 and the nominal plant composite bounds are generated at all designed frequencies. The objective of this bound is to ensure that the synthesized nominal open loop ($L_0(j\omega)$) lies on or just above the composite bound. The gain and phase contributions of the open loop transmission ($L_0(j\omega)$) at all designed frequencies that are obtained graphically to satisfy the robust stability, disturbance rejection, and tracking performance at each frequency are given in the Table S3 (Supporting Information). The objective function for the QFT bound index eq 47 is defined in such a way, that if the numerical value obtained from the algebraic representation of $L(j\omega)$ is the same as the graphically obtained value at all frequencies, respectively. J_{bi} is set to zero; otherwise, it represents the difference between the numerical and graphical obtained values. The control parameters of the PSO algorithm and initial penalty values of the objective function 44 are presented in Table S4 (Supporting Information).

The nominal loop transmission $L_0(s) = P_0(s)C(s)$ that satisfies all the bounds and stability contour is synthesized using modified PSO-enabled automatic loop shaping algorithm in the QFT environment (Figure 11). The corresponding current controller is synthesized for the exact amount of plant uncertainty, tracking, disturbance rejection, and stability

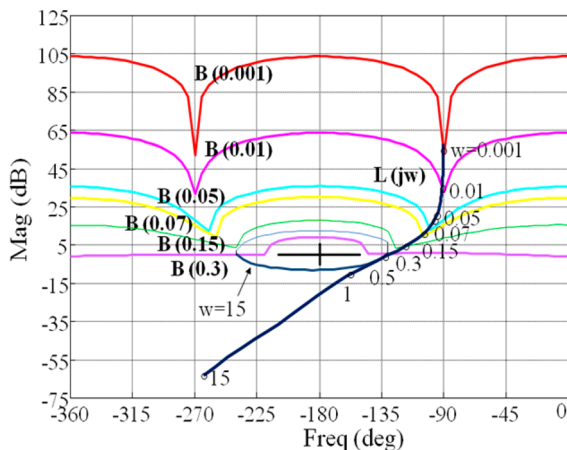


Figure 11. Loop shaping using PSO-enabled automated QFT.

specifications. The PSO algorithm converged to give the following robust controller

$$C(s) = \frac{13.41(s/36 + 1)}{(s/10 + 1)(s/80 + 1)} \quad (56)$$

The controller design has reduced the variations in the closed loop frequency response to the desired range. A prefilter is now required to achieve the required shape of the closed loop frequency response. The suitable prefilter, which satisfies tracking specifications perfectly, is

$$F(s) = \frac{s^2/0.63^2 + 0.89s/0.63 + 1}{(s/0.65 + 1)(s^2/1.17^2 + 1.52s/1.17 + 1)} \quad (57)$$

Figure 12 shows the Bode magnitude plot of the closed loop frequency response with a prefilter, together with the tracking frequency response specifications plotted with dashed lines.

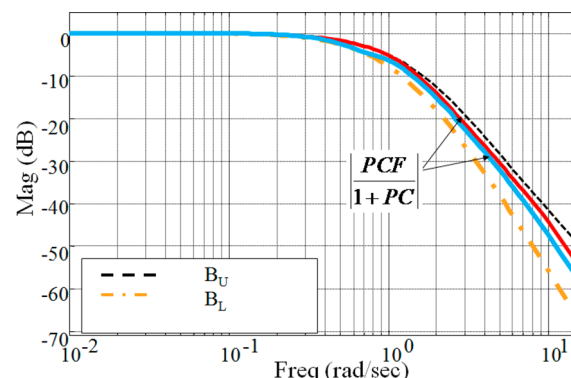


Figure 12. Closed loop frequency response with prefilter.

6.5. Design Validation and Discussion. The robust stability margin requirement should be checked first, and the result is shown in Figure 13. The worst case closed-loop

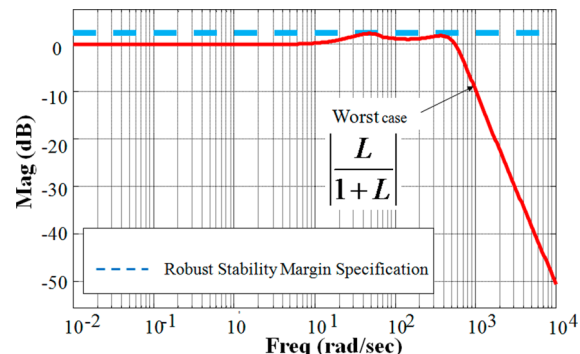


Figure 13. Validation of closed loop robust stability.

response magnitude (covering all uncertainty cases) is plotted in the solid line and, the design specification is plotted in the dotted line. The figure shows that the robust stability specification perfectly matches the desired stability value ($\mu = 1.3 = 2.3$ dB). Time domain simulation of the closed-loop system with the controller $C(s)$ and prefilter $F(s)$ (considering 378 plants within the uncertainty range) are shown in Figure 14, together with the tracking requirement (dashed line). The study has been conducted by keeping the set point at 50 degrees. It is evident from the figure that the designed current controller is quite capable of tracking the commanded reference

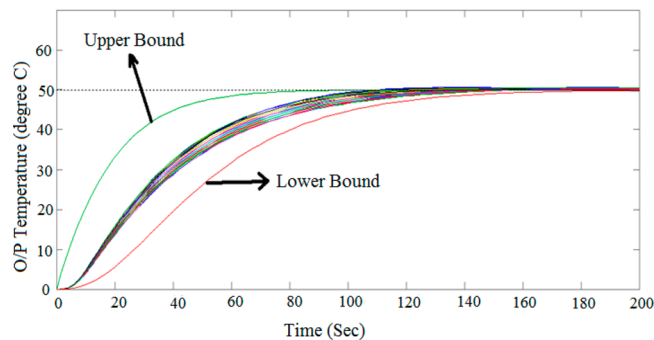


Figure 14. Step response (50 units) of the overall system with prefilter and controller.

temperature of the air preheating chamber despite some variations in operating conditions and operating regions. Figure 15 shows the variation of output temperature of model I

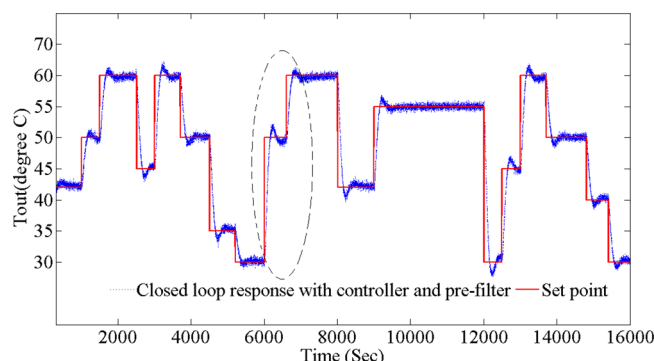


Figure 15. Closed loop response of the nominal plant (model I) with controller and prefilter.

(nominal plant) in a closed loop with the changes in furnace temperature setpoint. It can be observed from the figure that the process is subjected to a plant output disturbance due to changes in air flow setting, but it does not make any significant effect on furnace air setpoint tracking. To closely verify the performance of the designed controller in a closed loop, a section of the data obtained from Figure 15 was separately plotted in Figure 16. It is clearly noticeable from the figure that the rise time of the air preheating furnace for the closed loop setting is less than 200 s and the maximum overshoot is less than 2%. Therefore, it can be stated that satisfactory tracking performance was obtained with the proposed controller.

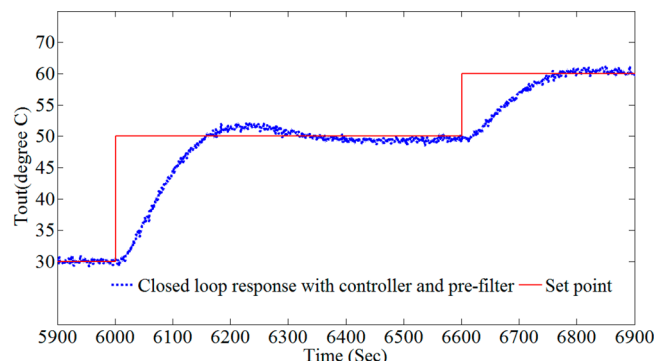


Figure 16. A section of the closed loop response shown in Figure 15.

Further, a comparative study between the proposed method (refined PSO-QFT) and two congruent automatic loop-shaping methods in QFT, namely, PSO-enabled QFT (PSO-QFT)^{55,79,80} and genetic algorithm (GA)-enabled QFT (GA-QFT)⁷² with other conventional PID tuning methods such as internal model control (IMC),⁹⁷ Cohen–Coon,⁹⁸ and Ziegler Nichols (ZN)⁹⁹ were performed in simulation to review the effectiveness of the proposed method over other similar and baseline methods. Figure 17 shows the response characteristics

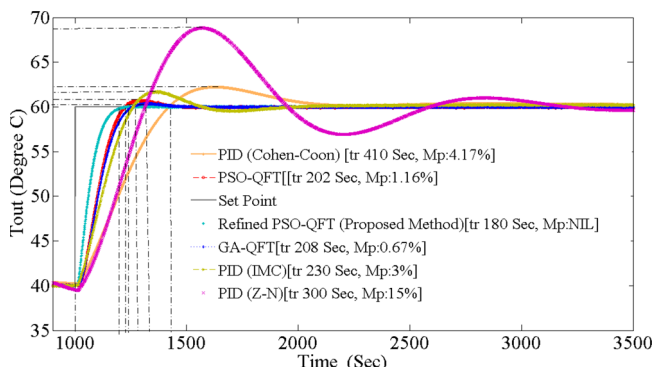


Figure 17. Comparative study in closed loop compensated time response (for worst case plant uncertainty) between the proposed method, PSO-QFT, GA-QFT, IMC, Cohen–Coon, and ZN methods.

of the worst case uncertain compensated system for a typical setpoint change (temperature setpoint changes from 40° to 60°) under these six different control methods. Various performance indicators like rise time (tr) and % peak overshoot (Mp) for each of the responses were also measured and presented in the same figure. The study clearly indicates that the current controller synthesized by the proposed method can achieve desired tracking performance specification acceptably, while other methods failed to bring the compensated response of the same worst case plant uncertainty within the requisite performance envelope. The simulation work as presented in Figure 17 has been extended in Figure 18 by considering the effect of flow disturbance (step) in addition to the existing simulation model. The aim of this study is to investigate the disturbance rejection performance of the proposed method over other methods. It is evident from Figure 18 that the disturbance rejection performance is much better with the

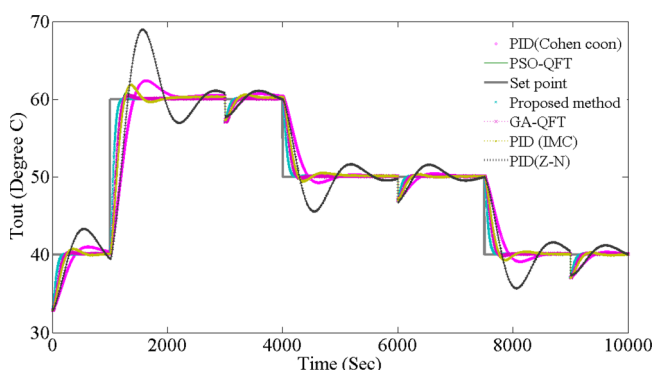


Figure 18. Comparison in disturbance rejection between the proposed method, PSO-QFT, GA-QFT, IMC, Cohen–Coon, and ZN methods.

proposed controller compared to the PSO-QFT, GA-QFT, PID (IMC), PID (Cohen–Coon), and PID (ZN) methods.

Further, to examine the performance of the proposed method under practical settings, the developed robust control law was implemented in LabVIEW¹⁰⁰ real-time environment through a PLC mod-bus interface, and the experimental results as obtained is presented in Figure 19. To collect the

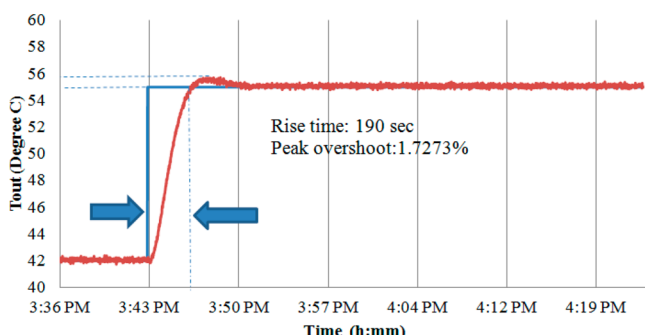


Figure 19. Experimental temperature response of the proposed controller implemented in LabVIEW real time environment through PLC mod-bus interface.

experimental data sets of the controlled process, at first the experimental setup was run under no-load for more than 1 h with a fixed temperature setting of 42 °C and flow setting of 100% (to eliminate the startup effect), then the temperature set point was changed to 55 °C by keeping flow settings unaltered. For comparison of the performance against a conventional controller, another experiment was performed with similar step input and operating and environmental conditions, with the autotuned PID controller of HC900 PLC, the results of which are presented in Figure 20. From the experimental response of

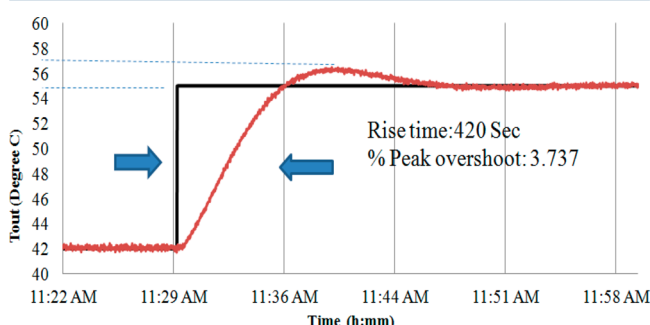


Figure 20. Experimental temperature response of the inbuilt autotuned PID controller of HC900 PLC.

the proposed controller as shown in Figure 19, the various performance measures like rise time and percentage peak overshoot were measured and found to be 190 seconds and 1.737%, respectively. The study clearly demonstrates that the measured performance indicators are reasonably correct and within the allowable tolerances of the performance specifications as given in eq 51. On the other hand, it can be observed from Figure 20 that the preheating chamber temperature response is much more sluggish with the inbuilt autotuned PID controller of HC900 PLC. Therefore, it can be stated that the proposed controller can provide much better performance compared to the exiting autotuned PID controller.

The present work has been formulated and tested on a scaled down model of an actual industrial system and found to provide

satisfactory results. But in a large-scaled industrial system, unmodeled dynamics may be significant and deteriorate the system performance. However, the control design method (QFT) that has been adopted in the present contribution can handle unstructured uncertainties as well.^{48,49,64} For the actual industrial process model, when unmodeled dynamics come into consideration that could well be treated as a disturbance to the uncertainty process model with the QFT design method. Therefore, in the actual industrial process some minor modifications are certainly needed in mathematical modeling and system identification as well as in control problem formulation, but the design philosophy will remain the same.

7. CONCLUSION

The paper has presented the modeling, identification, and control of the air preheating furnace of an industrial pneumatic conveying and drying system by using first-principles, system identification techniques, and a parametric robust control approach in a systematic manner. On the basis of the concept of one-dimensional forced convective heat transport phenomena, the first-principles models have been formulated. Then a set of accurate uncertainty process models for the various operating region and operating and environmental conditions was identified by using the simplified refined instrumental variable method for continuous-time (SRIVC) method. The model validation study reveals that the assumptions and approximations considered during formulation were reasonably correct, as the simulated model predicted response is quite close to the experimental model obtained results. The modeling strategies adopted in this paper also address how control-oriented modeling of complex systems can benefit from integrating first-principles and system identification methods. The identified uncertainty models have been used for robust controller design and implementation. The design problem with quantitative bounds on the plant templates and quantitative tolerances on the acceptable closed loop system response can easily be ascertained using the QFT feedback design. When the QFT controller was designed, a refined particle swarm optimization-enabled automated QFT (refined PSO-QFT) procedure was proposed, discussed, and employed to automate the loop shaping process. The automatic loop shaping using the refined PSO-QFT minimizes the trial and error involved in the manual synthesis of the nominal loop. The simulation study of the controlled process ensures a proper trade-off between required robust stability, satisfactory tracking, and disturbance rejection specifications in order to achieve the improved drying performance of the pneumatic drying and conveying system.

■ ASSOCIATED CONTENT

Supporting Information

Photograph of the experimental setup (Figure S1), SCADA implementation of process under investigations (Figure S2), performance measures of indentified models using testing data set (Table S1), search range of controller parameters during optimization process (Table S2), graphically obtained values of QFT bounds (Table S3), PSO and objective function parameters (Table S3). This material is available free of charge via the Internet at <http://pubs.acs.org>.

■ AUTHOR INFORMATION

Corresponding Author

*Tel.: +91-9434788130. E-mail: chiranjib_k@yahoo.com.

Notes

The authors declare no competing financial interest.

ACKNOWLEDGMENTS

This work has been supported by the Department of Science and Technology, Government of India (No. SR/FTP/ET A-02712009) and Department of Science and Technology, Government of West Bengal (No. 321(Sanc.)/ST/P/S&T/6G1/2010).

NOMENCLATURE

T_c =temperature of coil ($^{\circ}\text{C}$)

T_a =air temperature ($^{\circ}\text{C}$)

T_{ps} =steady state pipe temperature ($^{\circ}\text{C}$)

A_c =area per unit length [coil side] (m^2)

M_p =mass of pipe/furnace per unit length (kg/m)

M_c =mass of coil per unit length (kg/m)

$F=V^*M_a$ = mass flow rate of air ($\text{kg}\cdot\text{m}/\text{s}$)

α_c =heat transfer coefficient coil side ($\text{W}/(\text{m}^2\cdot\text{K})$)

C_p =specific heat of pipe ($\text{J}/(\text{kg}\cdot\text{K})$)

C_c =specific heat of coil ($\text{J}/(\text{kg}\cdot\text{K})$)

I =current input to heating coil (A)

τ_{pa} =heat flow time constant from pipe to air = ($M_p C_p / (\alpha_a A_a)$)

τ_c =time constant of heat flow through coil = ($M_c C_c / (\alpha_c A_c)$)

L =length of the pipe/furnace (m)

T_p =temperature of pipe ($^{\circ}\text{C}$)

T_{cs} =steady state coil temperature ($^{\circ}\text{C}$)

T_{as} =steady state air temperature ($^{\circ}\text{C}$)

A_a =area per unit length [Air flow side] (m^2)

M_a =mass of air per unit length (kg/m)

V =velocity of air flow (m/s)

v_s =steady state air flow velocity (m/s)

α_a =heat transfer coefficient air flow side ($\text{W}/(\text{m}^2\cdot\text{K})$)

C_a =specific heat of air ($\text{J}/(\text{kg}\cdot\text{K})$)

Q =heat input to heating coil (W)

τ_{cp} =heat flow time constant from coil to pipe = ($M_p C_p / (\alpha_c A_c)$)

τ_a =time constant of heat flow through air = ($M_a C_a / (\alpha_a A_a)$)

τ_{ca} =heat flow time constant from coil to air = ($M_a C_a / (\alpha_c A_c)$)

REFERENCES

- (1) Mills, David. *Pneumatic conveying Design Guide*; Butterworth-Heinemann: Oxford, UK, 2003.
- (2) Jangam, S. V.; Karthikeyan, M.; Mujumdar, A. S. A critical assessment of industrial coal drying technologies: Role of energy, emissions, risk and sustainability. *Dry. Technol.* **2011**, *29* (4), 395–407.
- (3) Bhattacharai, S.; Oh, J. H.; Euh, S. H.; Kim, D. H.; Yu, L. Simulation study for pneumatic conveying drying of sawdust for pellet production. *Dry. Technol.* **2014**, *32* (10), 1142–1156.
- (4) Kroehl, P.; Lindner, H. Method for the wet calcination of gypsum. U.S. Patent 5,437,850, 1995.
- (5) Rajan, K. S.; Srivastava, S. N.; Pitchumani, B.; Surendiran, V. Thermal conductance of pneumatic conveying preheater for air-gypsum and air-sand heat transfer. *Int. J. Therm. Sci.* **2010**, *49* (1), 182–186.
- (6) Erhard, H. S.; Korf, P.; Schneider, V. Process for the recycling of residues for the production of portland cement clinker. U.S. Patent No. 6,146,133, 2000.
- (7) Salvador, S.; Pons, O. A semi-mobile flash dryer/calciner unit to manufacture pozzolana from raw clay soils—Application to soil stabilisation. *Constr. Build. Mater.* **2000**, *14* (2), 109–117.
- (8) Warshawsky, J. Method of converting a rotary kiln cement making plant to a calcining furnace cement making plant. U.S. Patent No. 4,260,369, 1981.
- (9) Kaensup, W.; Kulwong, S.; Wongwises, S. A small-scale pneumatic conveying dryer of rough rice. *Dry. Technol.* **2006**, *24* (1), 105–113.
- (10) Vervaet, C.; Remon, J. P. Continuous granulation in the pharmaceutical industry. *Chem. Eng. Sci.* **2005**, *60* (14), 3949–3957.
- (11) Pelegrina, A. H.; Crapiste, G. H. Modelling the pneumatic drying of food particles. *J. Food Eng.* **2001**, *48* (4), 301–310.
- (12) Güner, M. Pneumatic conveying characteristics of some agricultural seeds. *J. Food Eng.* **2007**, *80* (3), 904–913.
- (13) Panchariya, P. C.; Popovic, D.; Sharma, A. L. Thin-layer modelling of black tea drying process. *J. Food Eng.* **2002**, *52* (4), 349–357.
- (14) Baker, C. G. J., Ed. *Industrial Drying of Foods*; Springer: New York, 1997.
- (15) Klinzing, G. E. *Pneumatic Conveying of Solids: A Theoretical and Practical Approach*; Springer: Dordrecht, The Netherlands, 1997.
- (16) Rajan, K. S.; Dhasandhan, K.; Srivastava, S. N.; Pitchumani, B. Studies on gas–solid heat transfer during pneumatic conveying. *Int. J. Heat Mass Transf.* **2008**, *51* (11), 2801–2813.
- (17) Radford, R. D. A model of particulate drying in pneumatic conveying systems. *Powder Technol.* **1997**, *93* (2), 109–126.
- (18) Mills, D.; Jones, M. G.; Agarwal, V. K. *Handbook of Pneumatic Conveying Engineering*; CRC Press: Boca Raton, FL, 2004.
- (19) Shvab, A. V.; Maltsev, A. A. Hydrodynamic model of pneumatic classification of powder materials. *Proc. 3rd Russ.-Korean Int. Symp. Sci. Technol.* **1999**, *2*, S18–S22.
- (20) Nakai, Y.; Senkawa, K.; Mishima, F.; Akiyama, Y.; Nishijima, S. High gradient magnetic separation of pneumatic conveyed powder products. *IEEE Trans. Appl. Supercond.* **2011**, *21* (3), 2063–2067.
- (21) Devahastin, S.; Mujumdar, A. S. Batch drying of grains in a well-mixed dryer-effect of continuous and stepwise change in drying air temperature. *Trans. ASAE* **1999**, *42* (2), 421–425.
- (22) Garcia, C. E.; Prett, D. M.; Morari, M. Model predictive control: Theory and practice—A survey. *Automatica* **1989**, *25* (3), 335–348.
- (23) Coelho, P. J. Mathematical modeling of the convection chamber of a utility boiler the theory. *Numer. Heat Trans. A, Appl.* **1999**, *36* (4), 429–447.
- (24) Roffel, B.; Rijnsdorp, J. E. Dynamics and control of a gas-fired furnace. *Chem. Eng. Sci.* **1974**, *29* (10), 2083–2092.
- (25) Tashtoush, B.; Molhim, M.; Al-Rousan, M. Dynamic model of an HVAC system for control analysis. *Energy* **2005**, *30* (10), 1729–1745.
- (26) Prívara, S.; Široký, J.; Ferkl, L.; Cigler, J. Model predictive control of a building heating system: The first experience. *Energy Buildings* **2011**, *43* (2), 564–572.
- (27) Saman, W.; Bruno, F.; Halawa, E. Thermal performance of PCM thermal storage unit for a roof integrated solar heating system. *Sol. Energy* **2005**, *78* (2), 341–349.
- (28) Rasmussen, B. P.; Alleyne, A. G.; Musser, A. B. Model-driven system identification of transcritical vapor compression systems. *IEEE Trans. Control Syst. Technol.* **2005**, *13* (3), 444–451.
- (29) Park, J. W.; Venayagamoorthy, G. K.; Harley, R. G. MLP/RBF neural-networks-based online global model identification of synchronous generator. *IEEE Trans. Ind. Electron.* **2005**, *52* (6), 1685–1695.
- (30) Xue, Z.; Lin, H.; Lee, T. H. Identification of Unknown Parameters for a Class of Two-Level Quantum Systems. *IEEE Trans. Autom. Control* **2013**, *58* (7), 1805–1810.
- (31) Cheng, S.; Zhang, P.; Habetsler, T. G. An impedance identification approach to sensitive detection and location of stator turn-to-turn faults in a closed-loop multiple-motor drive. *IEEE Trans. Ind. Electron.* **2011**, *58* (5), 1545–1554.
- (32) Wahab, N. A.; Katebi, R.; Balderud, J.; Rahmat, M. F. Data-driven adaptive model-based predictive control with application in wastewater systems. *IET Control Theory Appl.* **2011**, *5* (6), 803–812.

- (33) Na, X.; Zhang, Y.; Liu, Y.; Walcott, B. Nonlinear identification of laser welding process. *IEEE Trans. Control Syst. Technol.* **2010**, *18*, 927–934.
- (34) Thornhill, N. F.; Patwardhan, S. C.; Shah, S. L. A continuous stirred tank heater simulation model with applications. *J. Process Control* **2008**, *18* (3), 347–360.
- (35) Favoreel, W.; De Moor, B.; Van Overschee, P. Subspace state space system identification for industrial processes. *J. Process Control* **2000**, *10* (2), 149–155.
- (36) Seki, H.; Amano, S.; Emoto, G. Modeling and control system design of an industrial crystallizer train for *para*-xylene recovery. *J. Process Control* **2010**, *20* (9), 999–1008.
- (37) Romano, R. A.; Garcia, C. Valve friction and nonlinear process model closed-loop identification. *J. Process Control* **2011**, *21* (4), 667–677.
- (38) Sanchis, R.; Peñarrocha, I. Control of a ceramic tiles cooling process based on water spraying. *J. Process Control* **2009**, *19* (7), 1073–1081.
- (39) Sohlberg, B. Grey box modelling for model predictive control of a heating process. *J. Process Control* **2003**, *13* (3), 225–238.
- (40) Mohanty, S. Artificial neural network based system identification and model predictive control of a flotation column. *J. Process Control* **2009**, *19* (6), 991–999.
- (41) Kittisupakorn, P.; Thitiyasook, P.; Hussain, M. A.; Daosud, W. Neural network based model predictive control for a steel pickling process. *J. Process Control* **2009**, *19* (4), 579–590.
- (42) Tolmač, D.; Josimović, L.; Prvulović, S.; Dimitrijević, D. Experimental and numerical studies of heat transfer and kinetic drying of convection pneumatic dryer. *FME Trans.* **2011**, *39* (3), 139–144.
- (43) Tolmač, D.; Prvulović, S.; Radovanović, L. Effects of heat transfer on convection dryer with pneumatic transport of material. *FME Trans.* **2008**, *36* (1), 45–49.
- (44) Li, J.; Mason, D. J. A computational investigation of transient heat transfer in pneumatic transport of granular particles. *Powder Technol.* **2000**, *112* (3), 273–282.
- (45) Sheng, Y. Y.; Irons, G. A. Mathematical and physical modelling of fluid flow and heat transfer in electric smelting. *Can. Metall. Quart.* **1998**, *37* (3–4), 265–273.
- (46) Bezuidenhout, J. J.; Eksteen, J. J.; Bradshaw, S. M. Computational fluid dynamic modelling of an electric furnace used in the smelting of PGM containing concentrates. *Miner. Eng.* **2009**, *22* (11), 995–1006.
- (47) Hansen, L. P.; Sargent, T. J. Robust control and model uncertainty. *Am. Econ. Rev.* **2001**, *60*–66.
- (48) Horowitz, I. M. *Quantitative feedback design*; QFT Publications: Boulder, CO, 1993.
- (49) Yaniv, Oded. *Quantitative Feedback Design of Linear and Nonlinear Control Systems*. Springer: New York, 1999.
- (50) Wu, S. F.; Grindle, M. J.; Breslin, S. G. Introduction to quantitative feedback theory for lateral robust flight control systems design. *Control Eng. Pract.* **1998**, *6* (7), 805–828.
- (51) Wu, S. F.; Grindle, M. J.; Wei, W. QFT based robust/fault tolerant flight control design for a remote pilotless vehicle. *Proc. 1999 IEEE Int. Conf. Control Appl.* **1999**, *1*, 57–62.
- (52) Karpenko, M.; Sepehri, N. Electrohydraulic force control design of a hardware-in-the-loop load emulator using a nonlinear QFT technique. *Control Eng. Pract.* **2012**, *20* (6), 598–609.
- (53) Desanj, D. S.; Grindle, M. J. Design of a marine autopilot using quantitative feedback theory. *Proc. 1998 Am. Control Conf.* **1998**, *1*, 384–388.
- (54) Satpati, B.; Sadhu, S. Course changing control for a cargo mariner class ship using quantitative feedback theory. *IE (I), Mar. Div. J.* **2008**, *88*, 1–8.
- (55) Satpati, B.; Bandyopadhyay, I.; Koley, C.; Ojha, S. K. Robust controller design for course changing/course keeping control of a ship using PSO enabled automated quantitative feedback theory. *IEEE Region 10 Conf.-TENCON 2008*, 1–6.
- (56) Benshabat, D. G.; Chait, Y. Application of quantitative feedback theory to a class of missiles. *J. Guid. Control Dyn.* **1993**, *16* (1), 47–52.
- (57) Ma, S. S.; Zhang, J. W.; Chai, S. C.; Feng, J. Application of QFT for missile flight control. *Trans. Beijing Inst. Technol.* **2013**, *33* (2), 155–159.
- (58) Reddi, Y.; Boje, E. Disturbance rejection design for a bank-to-turn missile using decoupling quantitative feedback theory. *Robust Control Design* **2012**, *7* (1), 139–144.
- (59) Khodabakhshian, A.; Hemmati, R. Robust decentralized multi-machine power system stabilizer design using quantitative feedback theory. *Int. J. Elec. Power* **2012**, *41* (1), 112–119.
- (60) Khodabakhshian, A.; Mahdianpoor, M.; Hooshmand, R. A. Robust control design for multi-functional DVR implementation in distribution systems using quantitative feedback theory. *Electr. Pow. Syst. Res.* **2013**, *97*, 116–125.
- (61) Shrikant Rao, P.; Sen, I. Robust tuning of power system stabilizers using QFT. *IEEE Trans. Control Syst. Technol.* **1999**, *7* (4), 478–486.
- (62) Olalla, C.; Carrejo, C.; Leyva, R.; Alonso, C.; Estibals, B. Digital QFT robust control of DC–DC current-mode converters. *Electr. Eng.* **2013**, *95* (1), 21–31.
- (63) Choi, S. B.; Cho, S. S.; Shin, H. C.; Kim, H. K. Quantitative feedback theory control of a single-link flexible manipulator featuring piezoelectric actuator and sensor. *Smart Mater. Struct.* **1999**, *8* (3), 338.
- (64) Rober, S. J.; Shin, Y. C.; Nwokah, O. D. I. A digital robust controller for cutting force control in the end milling process. *J. Dyn. Syst-T ASME* **1997**, *119* (2), 146–152.
- (65) Wang, Z.; Chen, Z.; Sun, Q.; Yuan, Z. Multivariable decoupling predictive control based on QFT theory and application in CSTR chemical process. *Chin. J. Chem. Eng.* **2006**, *14* (6), 765–769.
- (66) Alavi, S. M.; Saif, M. A QFT-based decentralized design approach for integrated fault detection and control. *IEEE Trans. Control Syst. Technol.* **2012**, *20* (5), 1366–1375.
- (67) Borghesani, C.; Chait, Y.; Yaniv, O. *Quantitative Feedback Theory Toolbox for Use with MATLAB: User's Guide*. MathWorks, Incorporated, 1994.
- (68) Zolotas, A. C.; Halikias, G. D. Optimal design of PID controllers using the QFT method. *IEE Proc. Control Theor. Appl.* **1999**, *146* (6), 585–589.
- (69) Gera, A.; Horowitz, I. Optimization of the loop transfer function. *Int. J. Control.* **1980**, *31* (2), 389–398.
- (70) Ballance, D. J.; Gawthrop, P. J. Control systems design via a quantitative feedback theory approach. *Int. Conf. Control 1991* **1991**, 476–480.
- (71) Thompson, D. F.; Nwokah, O. D. Analytic loop shaping methods in quantitative feedback theory. *J. Dyn. Syst-T ASME* **1994**, *116* (2), 169–177.
- (72) Chen, W. H.; Ballance, D. J.; Feng, W.; Li, Y. Genetic algorithm enabled computer-automated design of QFT control systems. *Proc. 1999 IEEE Int. Symp. Comput. Aid. Control Syst. Des.* **1999**, 492–497.
- (73) Cervera, J.; Baños, A. Automatic loop shaping in QFT by using CRONE structures. *Fract. Differ. Appl.* **2006**, *2* (1), 207–212.
- (74) Patil, M. D.; Nataraj, P. S. V.; Vyawahare, V. A. Automated design of fractional PI QFT controller using interval constraint satisfaction technique (ICST). *Nonlinear Dyn.* **2012**, *69* (3), 1405–1422.
- (75) Cervera, J.; Baños, A. Automatic loop shaping in QFT using CRONE structures. *J. Vib. Control* **2008**, *14* (9–10), 1513–1529.
- (76) SV Paluri, N.; Kubal, N. Automatic loop shaping in QFT using hybrid optimization and constraint propagation techniques. *Int. J. Robust Nonlin.* **2007**, *17* (2–3), 251–264.
- (77) Nataraj, P. S. V.; Deshpande, M. M. Automated synthesis of fixed structure QFT controller using interval constraint satisfaction techniques. In Proceedings of the 17th World Congress, The International Federation of Automatic Control, Seoul, Korea, 2008; pp 4976–4981.
- (78) Patil, M. D.; Nataraj, P. S. V. Automated synthesis of multivariable QFT controller using interval constraint satisfaction technique. *J. Process Control* **2012**, *22* (4), 751–765.
- (79) Satpati, B.; Bandyopadhyay, I.; Das, G.; Koley, C. Robust controller design for load frequency control of non-minimum phase

- Hydro power plant using PSO enabled automated Quantitative Feedback Theory. *Ann. IEEE India Conf.* 2008, 2, 349–354.
- (80) Satpati, B.; Koley, C.; Datta, S. Robust PID controller design using PSO enabled automated QFT approach for first order lag system with minimal dead time. *Syst. Sci. Control Eng.: Open Access J.* 2014, DOI: 10.1080/21642583.2014.912570.
- (81) Tan, K. C.; Lee, T. H.; Khor, E. F. Automatic design of multi-variable quantitative feedback theory control systems via evolutionary computation. *P. I. Mech. Eng. I, J. Sys.* 2001, 215 (3), 245–259.
- (82) Kennedy, James. Particle swarm optimization. In *Encyclopedia of Machine Learning*; Springer: New York, 2010; pp 760–766.
- (83) Castano, J. E.; Patino, J. A.; Espinosa, J. J. Model identification for control of a distillation column. Robotics Symposium, 2011 IEEE IX Latin American and IEEE Colombian Conference on Automatic Control and Industry Applications (LARC), Bogota, Oct 1–4, 2011; pp 1–5.
- (84) Lienhard, J. H. *A Heat Transfer Textbook*; Courier Dover Publications: Mineola, NY, 2011.
- (85) Satpati, B.; Alam, M. A.; Datta, S.; Koley, C. Modelling simulation and validation of duct air heating system. In Proceedings of the 2013 IEEE International Conference on Control Applications (CCA), Hyderabad, India, IEEE, 2013; pp 1061–1068.
- (86) Ljung, Lennart. Experiments with identification of continuous time models. In proceedings of the 15th IFAC Symposium on System Identification, Saint-Malo, France, 2009.
- (87) Garnier, H.; Gilson, M.; Bastogne, T.; Mensler, M. *The CONTSID Toolbox: A Software Support for Data-Based Continuous-Time Modeling*; Springer: London, 2008; pp 249–290.
- (88) Garnier, H.; Mensler, M. The CONTSID toolbox: a matlab toolbox for CONTinuous-Time System IDentification. In Proceedings of the 12th IFAC Symposium on System Identification, Santa Barbara, USA, 2000.
- (89) Garnier, H.; Gilson, M.; Laurain, V.; Ni, B. Developments for the CONTSID toolbox. *Syst. Identif.* 2012, 16 (1), 1553–1558.
- (90) Ljung, Lennart. *The System Identification Toolbox: The Manual*, 1st ed.; The Math Works Inc.: Natick MA, 1986; 7th ed., 2007.
- (91) Garnier, H.; Gilson, M.; Young, P. C.; Huselstein, E. An optimal IV technique for identifying continuous-time transfer function model of multiple input systems. *Control Eng. Pract.* 2007, 15 (4), 471–486.
- (92) Gu, J.; Taylor, J.; Seward, D. Modelling of an hydraulic excavator using the simplified refined instrumental variable (SRIV) algorithm. *J. Control Theory Appl.* 2007, 5 (4), 391–396.
- (93) Garnier, H.; Young, P. Time-domain approaches to continuous-time model identification of dynamical systems from sampled data. In Proceeding of the 2004 American Control Conference, Boston, MA, 2004.
- (94) Zajic, I.; Larkowski, T.; Burnham, K. J.; Hill, D. Control analysis and tuning of an industrial temperature control system. *Adv. PID Control* 2012, 2 (1), 679–684.
- (95) Yeniyay, O. Penalty function methods for constrained optimization with genetic algorithms. *Math. Comput. Appl.* 2005, 10 (1), 45–56.
- (96) Lam, J. Model reduction of delay systems using Padé approximants. *Int. J. Control.* 1993, 57 (2), 377–391.
- (97) Chien, I. L. IMC-PID controller design—An extension. *2nd Int. IFAC Symp.* 1988, 147–152.
- (98) Ziegler, J. G.; Nichols, N. B. Optimum settings for automatic controllers. *Trans. ASME* 1942, 64(11).
- (99) Cohen, G.; Coon, G. A. Theoretical consideration of retarded control. *Trans. ASME* 1953, 75 (1), 827–834.
- (100) Manual, LabVIEW User. National Instruments: Austin, TX, 1998.